



HAL
open science

An extreme blue nugget, UV-bright starburst at $z = 3.613$ with 90 per cent of Lyman continuum photon escape

R. Marques-Chaves, D. Schaerer, J. Álvarez-Márquez, A. Verhamme, D. Ceverino, J. Chisholm, L. Colina, M. Dessauges-Zavadsky, I. Pérez-Fournon, A. Saldana-Lopez, et al.

► To cite this version:

R. Marques-Chaves, D. Schaerer, J. Álvarez-Márquez, A. Verhamme, D. Ceverino, et al.. An extreme blue nugget, UV-bright starburst at $z = 3.613$ with 90 per cent of Lyman continuum photon escape. *Monthly Notices of the Royal Astronomical Society*, 2022, 517, pp.2972-2989. 10.1093/mnras/stac2893 . insu-03867371

HAL Id: insu-03867371

<https://insu.hal.science/insu-03867371>

Submitted on 11 Apr 2023

HAL is a multi-disciplinary open access archive for the deposit and dissemination of scientific research documents, whether they are published or not. The documents may come from teaching and research institutions in France or abroad, or from public or private research centers.

L'archive ouverte pluridisciplinaire **HAL**, est destinée au dépôt et à la diffusion de documents scientifiques de niveau recherche, publiés ou non, émanant des établissements d'enseignement et de recherche français ou étrangers, des laboratoires publics ou privés.

An extreme blue nugget, UV-bright starburst at $z = 3.613$ with 90 per cent of Lyman continuum photon escape

R. Marques-Chaves ¹★, D. Schaerer,^{1,2} J. Álvarez-Márquez,³ A. Verhamme,¹ D. Ceverino ^{4,5},
J. Chisholm ⁶, L. Colina,^{3,7} M. Dessauges-Zavadsky ¹, I. Pérez-Fournon,^{8,9} A. Saldana-Lopez ¹,
A. Upadhyaya¹ and E. Vanzella¹⁰

¹Geneva Observatory, Department of Astronomy, University of Geneva, Chemin Pegasi 51, CH-1290 Versoix, Switzerland

²CNRS, IRAP, 14 Avenue E. Belin, F-31400 Toulouse, France

³Centro de Astrobiología (CSIC-INTA), Carretera de Ajalvir, E-28850 Torrejón de Ardoz, Madrid, Spain

⁴Universidad Autónoma de Madrid, Ciudad Universitaria de Cantoblanco, E-28049 Madrid, Spain

⁵CIAFF, Facultad de Ciencias, Universidad Autónoma de Madrid, E-28049 Madrid, Spain

⁶Department of Astronomy, The University of Texas at Austin, 2515 Speedway, Stop C1400, Austin, TX 78712-1205, USA

⁷International Associate, Cosmic Dawn Center (DAWN)

⁸Instituto de Astrofísica de Canarias, C/Vía Láctea, s/n, E-38205 San Cristóbal de La Laguna, Tenerife, Spain

⁹Dpto. Astrofísica, Universidad de La Laguna, E-38206 San Cristóbal de La Laguna, Tenerife, Spain

¹⁰INAF - OAS, Osservatorio di Astrofisica e Scienza dello Spazio di Bologna, via Gobetti 93/3, I-40129 Bologna, Italy

Accepted 2022 October 5. Received 2022 October 4; in original form 2022 July 25

ABSTRACT

We present the discovery and analysis of J1316+2614 at $z = 3.6130$, a UV-bright star-forming galaxy ($M_{UV} \simeq -24.7$) with large escape of Lyman continuum (LyC) radiation. J1316+2614 is a young ($\simeq 10$ Myr) star-forming galaxy with $SFR \simeq 500 M_{\odot} \text{ yr}^{-1}$ and a starburst mass of $\log(M_{\star}/M_{\odot}) \simeq 9.7$. It shows a very steep UV continuum, $\beta_{UV} = -2.59 \pm 0.05$, consistent with residual dust obscuration, $E(B - V) \simeq 0$. LyC emission is detected with high significance ($\simeq 17\sigma$) down to 830 \AA , for which a very high relative (absolute) LyC escape fraction $f_{\text{esc}}(\text{LyC}) \simeq 0.92$ ($\simeq 0.87$) is inferred. The contribution of a foreground or active galactic nucleus contamination to the LyC signal is discussed, but is unlikely. J1316+2614 is the most powerful ionizing source known among the star-forming galaxy population, both in terms of production ($Q_{\text{H}} \approx 10^{56} \text{ s}^{-1}$) and escape of ionizing photons ($f_{\text{esc}}(\text{LyC}) \approx 0.9$). Nebular emission in Ly α , H β , and other rest-frame optical lines are detected, but these are weak ($E W_0[\text{H}\beta] \simeq 35 \text{ \AA}$), with their strengths reduced roughly by $\simeq 90$ per cent. J1316+2614 is the first case known where the effect of large escape of ionizing photons on the strength of nebular lines and continuum emission is clearly observed. Gas inflows are detected in J1316+2614 from the blue-dominated peak Ly α emission (with a blue-to-red peak line ratio $I_{\text{blue}}/I_{\text{red}} \simeq 3.7$) and redshifted interstellar medium absorption ($\simeq 100 \text{ km s}^{-1}$). Our results suggest that J1316+2614 is undergoing a gas compaction event, possibly representing a short-lived phase in the evolution of massive and compact galaxies, where strong gas inflows have triggered an extreme star formation episode and nearly 100 per cent LyC photons are escaping.

Key words: galaxies: evolution – galaxies: formation – galaxies: high-redshift.

1 INTRODUCTION

One of the key questions of modern observational cosmology is to identify the sources responsible for the ionization of the neutral intergalactic medium (IGM) in the first Gyr of cosmic time – the Epoch of Reionization (EoR). It is widely recognized from various observations that the EoR happened at $z \sim 6\text{--}15$ (e.g. Bañados et al. 2018; Mason et al. 2018; Planck Collaboration VI 2020), yet the sources that were responsible for the majority of ionizing photons (with $> 13.6 \text{ eV}$; hereafter Lyman continuum, LyC) remain elusive.

Faint star-forming galaxies are thought to be the main drivers for reionization (see e.g. Robertson et al. 2015; Finkelstein et al. 2019) due to their high number density. Also, these sources may

have higher ionizing photon production efficiency (ξ_{ion} , e.g. Schaerer et al. 2016; Maseda et al. 2020) compared to UV-bright, massive counterparts. However, LyC surveys of faint star-forming galaxies at $z \lesssim 4$, where LyC radiation can be directly observed and measured, have revealed relatively low or negligible LyC escape fractions on average ($f_{\text{esc}}(\text{LyC}) \lesssim 0.1$; e.g. Marchi et al. 2017; Rutkowski et al. 2017; Fletcher et al. 2019; Bian & Fan 2020; Flury et al. 2022a). Only for a few individual galaxies LyC is detected with high significance and large LyC escape fractions are inferred ($f_{\text{esc}}(\text{LyC}) \geq 0.2$; e.g. de Barros et al. 2016; Vanzella et al. 2016; Izotov et al. 2018a,b; Steidel et al. 2018; Fletcher et al. 2019; Flury et al. 2022a).

Dedicated surveys have been also carried out to investigate the properties of these sources and understand the main mechanisms for LyC leakage (e.g. Steidel et al. 2018; Fletcher et al. 2019; Flury et al. 2022a). Despite these huge observational efforts, the connection between LyC leakage and different galaxy properties is still not fully

* E-mail: ruijmcoelho@gmail.com

understood. Some properties appear to correlate with LyC leakage. UV compact morphologies and large star formation surface densities (ΣSFR), low dust attenuation, low covering fraction of gas, and high-ionization parameters among others appear to be common in strong LyC emitters (e.g. Jaskot & Oey 2013; Alexandroff et al. 2015; Sharma et al. 2016; Izotov et al. 2018a; Flury et al. 2022b; Saldana-Lopez et al. 2022). On the other hand, other properties appear to not correlate at all or show weak correlation only, including the stellar mass, metallicity, or spectral hardness (e.g. Flury et al. 2022b; Marques-Chaves et al. 2022; Saxena et al. 2022). Motivated by these findings and other empirical trends, indirect tracers of LyC leakage have been proposed, tested, and some of them successfully established (e.g. Zackrisson, Inoue & Jensen 2013; Nakajima & Ouchi 2014; Verhamme et al. 2015; Sharma et al. 2017; Chisholm et al. 2018, 2022; Izotov et al. 2018b; Saldana-Lopez et al. 2022; Schaerer et al. 2022; Xu et al. 2022). These can be used at all redshifts including in the EoR, where the detection of LyC is statistically unlikely due to the opacity of the IGM (Inoue et al. 2014).

On the opposite side of the UV luminosity function are the more rare, UV-bright star-forming galaxies. By definition, these sources probe intense star formation and therefore high production of ionizing photons. Recent works have found remarkably luminous star-forming galaxies at $z > 6$ (e.g. Hashimoto et al. 2019; Morishita et al. 2020; Endsley et al. 2021; Bouwens et al. 2022a), including the highest spectroscopically and photometrically redshift sources known, leading to important implications (Oesch et al. 2016; Harikane et al. 2022b). The volume density inferred for these luminous sources is much higher than that predicted by models (e.g. Mason et al. 2018), by factors of ~ 10 –100. Active galactic nucleus (AGN) contamination could be a natural explanation for the excess of UV-bright sources in the early Universe, but recent results disfavour such scenario (Finkelstein & Bagley 2022). Rather than that, higher star formation efficiency than previously thought at early times and/or lower dust obscuration towards the UV-bright end of luminosity functions are invoked (e.g. Yung et al. 2019; Harikane et al. 2022a). Also, it has been shown that there is little or no evolution in the number density of very bright sources ($M_{\text{UV}} \simeq -23$) between $z = 4$ and $z = 10$ (e.g. Bowler et al. 2020; Harikane et al. 2022a), implying that the relative number of UV-bright to UV-faint sources increases towards higher redshifts. However, the number of UV-bright sources is still scarce and their space density highly uncertain, ranging from $\lesssim 10^{-7}$ to some 10^{-6} Mpc^{-3} for $M_{\text{UV}} \simeq -23$ at $z \simeq 7$ –8 (e.g. Calvi et al. 2016; Bowler et al. 2020; Rojas-Ruiz et al. 2020; Leethochawalit et al. 2022), possibly reflecting cosmic variance effects. While a precise determination of the number density of these EoR bright sources can be done with the upcoming very wide surveys like *Euclid* and *Nancy Grace Roman Space Telescope*, other important questions remain to be answered: what role do these UV-bright sources have to galaxy formation and evolution, and to cosmic reionization?

Recently, we have undertaken a search for very luminous star-forming galaxies at $z \gtrsim 2$ within the $\sim 9000 \text{ deg}^2$ -wide extended Baryon Oscillation Spectroscopic Survey (eBOSS Abolfathi et al. 2018) of the Sloan Digital Sky Survey (SDSS; Eisenstein et al. 2011). The first results of this project were presented in Marques-Chaves et al. (2020b), Álvarez-Márquez et al. (2021), and Marques-Chaves et al. (2021), where two UV-bright ($M_{\text{UV}} < -24$) star-forming galaxies were analysed in detail, BOSS-EUVLG1 at $z = 2.47$ and J0121+0025 at $z = 3.24$. These sources are very young ($\lesssim 10 \text{ Myr}$) and compact ($r_{\text{eff}} \sim 1 \text{ kpc}$) starbursts with star formation rates $\text{SFR} \simeq 1000 \text{ M}_{\odot} \text{ yr}^{-1}$, but with low dust attenuation ($E(B -$

$V) \lesssim 0.1$). For example, dust is not detected in BOSS-EVULG1, yielding a dust mass $\log(M_{\text{dust}}/M_{\odot}) < 7.3$ and a dust to stellar mass ratio $M_{\text{dust}}/M_{\star} \simeq 2 \times 10^{-3}$ (Marques-Chaves et al. 2020b). While no direct information on the LyC leakage is known for BOSS-EUVLG1, J0121+0025 shows significant emission below the Lyman edge, compatible with large $f_{\text{esc}}(\text{LyC}) \approx 40$ per cent (Marques-Chaves et al. 2021), implying that that UV-bright galaxies can emit ionizing photons. The spectral energy distributions (SED) of these sources are fully dominated by the young starburst with specific SFR of $s\text{SFR} \sim 100 \text{ Gyr}^{-1}$, and without a relevant old stellar component, possibly indicating that the bulk of their stellar mass ($\simeq 10^{10} M_{\odot}$) was assembled in a few Myr. All together, these authors speculate that these rare UV-bright starbursts ($\sim 10^{-9} \text{ Mpc}^{-3}$, Marques-Chaves et al. 2020b) could represent an early and short-lived phase in the evolution of massive galaxies, such as compact ellipticals or dusty star-forming galaxies found at $z \simeq 2$ –3. However, the main mechanism and physical conditions behind the formation of such extreme starbursts are not understood yet.

In this work, we present SDSS J131629.61+261407.0 at $z = 3.6130$ (α, δ [J2000] = 199.1234°, 26.2353°, hereafter J1316+2614). J1316+2614 is a very luminous ($M_{\text{UV}} = -24.6$) star-forming galaxy with $\simeq 90$ per cent LyC leakage and signatures of inflowing gas, shedding further light on the physical mechanism of galaxy formation of these peculiar UV-bright sources. The paper is structured as follows. The discovery and follow-up observations are presented in Section 2. The analysis of the rest-frame UV spectroscopic observations, including the ionizing and non-ionizing spectra of J1316+2614, is presented in Section 3. In Section 4, we discuss the properties of J1316+2614 and compare them with those from other sources in the literature. Finally, we present the summary of our main findings in Section 5. Throughout this work, we assume concordance cosmology with $\Omega_{\text{m}} = 0.274$, $\Omega_{\Lambda} = 0.726$, and $H_0 = 70 \text{ km s}^{-1} \text{ Mpc}^{-1}$. Magnitudes are given in the AB system. Absolute magnitudes and luminosities are not corrected by dust.

2 DISCOVERY AND FOLLOW-UP OBSERVATIONS

J1316+2614 at $z = 3.613$ was discovered as part of our search for luminous star-forming galaxies at high redshift ($z > 2$) within the $\sim 9300 \text{ deg}^2$ -wide eBOSS/SDSS (Eisenstein et al. 2011; Abolfathi et al. 2018). Similar as BOSS-EUVLG1 and J0121+0025 (Marques-Chaves et al. 2020b, 2021), J1316+2614 is classified as a quasi-stellar object (QSO) in the Data Release 14 Quasar catalogue (Pâris et al. 2018), but its BOSS spectrum (plate-mjd-fiberid: 5997-56309-375)¹ shows features characteristic of a young star-forming galaxy, without any hint of AGN activity. It shows narrow Ly α emission (a full width at half-maximum, FWHM, of $\simeq 500 \text{ km s}^{-1}$) and P-Cygni features in the wind lines N V 1240 Å and C IV 1550 Å, which is indicative of a young stellar population. Moreover, J1316+2614 shows a compact morphology without any evidence of being magnified by gravitational lensing, such as multiple images or arc-like morphologies, or the presence of nearby bright lens (Fig. 1).

2.1 Optical observations

We obtained optical spectra of J1316+2614 with the Optical System for Imaging and low-Intermediate-Resolution Integrated Spec-

¹<http://skyserver.sdss.org/dr14/en/tools/explore/summary.aspx?id=1237667442439750118>

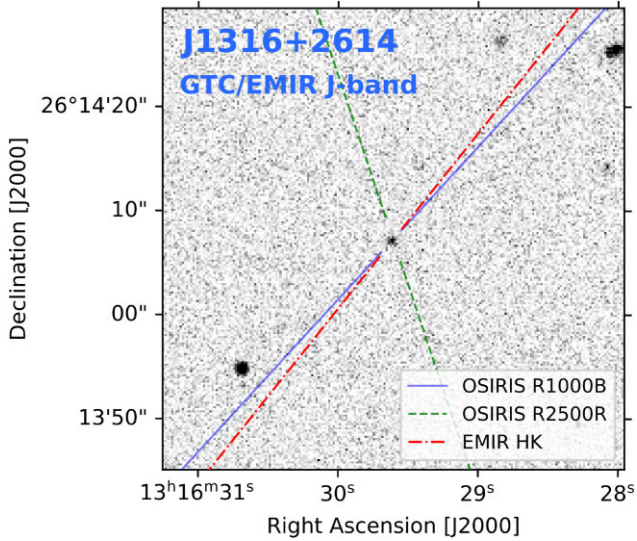


Figure 1. Cut-out of J1316+2614 from the GTC/EMIR *J*-band image. J1316+2614 is located in the centre of the image. The orientation of the GTC long-slits is marked in blue (solid), green (dashed), and red (dash-dot) lines for the optical OSIRIS low-resolution (R1000B), medium-resolution (R2500R), and near-IR EMIR (HK) grisms, respectively.

troscopy instrument (OSIRIS)² on the 10.4m Gran Telescopio Canarias (GTC) telescope as part of the programs GTCMULTIPLE2F-18A and GTC29-21A (PI: R. Marques-Chaves). OSIRIS observations were performed under $\simeq 0.9$ – 1.1 arcsec seeing conditions (FWHM) using the R2500R and R1000B grisms providing spectral resolutions $R \sim 1800$ and $R \sim 700$ and coverage of 5580–7700 and 3600–7600 Å, respectively. Long-slits with 1.0 arcsec-width were centred on J1316+2614 and oriented with the parallactic angle (Fig. 1). Total on-source exposure times are 150 and 60 min for the medium and low-resolution observations, respectively. Table 1 summarizes the GTC spectroscopic observations.

Data were reduced following standard reduction procedures using IRAF. These include subtraction of the bias and further correction of the flat-field. The wavelength calibration is done using HgAr+Ne+Xe arc lamps data. 2D spectra are background subtracted using sky regions around J1316+2614. Individual 1D spectra are extracted, stacked, and corrected for the instrumental response using observations of the standard star Ross 640. We use the extinction curve of Cardelli, Clayton & Mathis (1989) and the extinction map of Schlafly & Finkbeiner (2011) to correct for the reddening effect in the Galaxy. Finally, the flux of the spectrum is matched to that obtained from photometry in the *R* band to account for slit-losses, and corrected for telluric absorption using the IRAF *telluric* routine.

2.2 Near-IR observations

Near-IR spectra were obtained with the Espectrógrafo Multiobjeto Infra-Rojo (EMIR)³ on the GTC under good seeing conditions (0.7 arcsec FWHM). The *HK* grism with a 0.8 arcsec-width was used with a total observing time of 43 min with a standard 10 arcsec ABBA dither, providing a spectral resolution $R \sim 700$ and coverage of 1.45–2.41 μm . Reduction of the near-IR spectrum was performed

using the official EMIR pipeline.⁴ Spectra were flux calibrated using a standard star observed in that night, and fluxes matched to those obtained from photometry. We also obtained near-IR imaging with EMIR using the *Y*, *J*, *H*, and *K_s* filters (Fig. 1). Total exposure times range from $\simeq 10$ to $\simeq 30$ min. Images were also reduced using the EMIR pipeline and were flux calibrated against 2MASS stars in the field. J1316+2614 is detected with high significance in all near-IR bands and appears unresolved in these images with seeing conditions $\simeq 0.9$ – 1.1 arcsec FWHM.

3 RESULTS

3.1 Rest-frame UV spectrum and young stellar population

The OSIRIS/GTC medium-resolution spectrum of J1316+2614 is shown in Fig. 2. It shows a blue UV continuum with a slope, -2.59 ± 0.05 , measured using two spectral windows of 30 Å-width at 1300 and 1600 Å rest frame and assuming that $F_{\lambda} \propto \lambda^{\beta_{UV}}$. This is steeper, but consistent within the uncertainties, than the slope derived from the photometry using *i* and *J* bands, $\beta_{UV}^{\text{phot}} = -2.43 \pm 0.17$, which probes slightly longer wavelengths of $\simeq 1600$ to $\simeq 2700$ Å (rest frame).

The most prominent features in the UV spectrum of J1316+2614 are the strong P-Cygni profiles seen in stellar wind lines. In particular, the profiles of N V 1240 Å and C IV 1550 Å are known to be strongly dependent on the age and metallicity of the stellar population (e.g. Chisholm et al. 2019). To investigate these properties, we compare the observed N V and C IV profiles to those obtained with the spectral synthesis code STARBURST99 (S99; Leitherer et al. 1999), following the same methodology described in Marques-Chaves et al. (2018) and Marques-Chaves et al. (2020a). S99 models are preferred in this fit instead of BPASS ones (Stanway, Eldridge & Becker 2016), because the shape of the P-Cygni absorption of C IV in the latter is difficult to match with observations (see discussion in Steidel et al. 2016). The effect of binary stars contributing to the spectrum of J1316+2614 will be discussed in Section 4.3.

We generate UV spectra using standard Geneva tracks with a grid of metallicities (Z_{*}/Z_{\odot} , where we assume $Z_{\odot} = 0.02$) of 0.05, 0.2, 0.4, and 1. We assume both continuous and burst star formation histories and an initial mass function with a power slope index $\alpha = -2.35$ over the mass range $0.5 < M_{*}/M_{\odot} < 100$. A χ^2 minimization is performed in the continuum normalized profiles of N V and C IV over the spectral ranges 1227–1246 and 1526–1545 Å, respectively. For C IV, we avoid fitting regions > 1545 Å as they include the interstellar component of C IV that is redshifted by $\simeq 100$ km s⁻¹ (see Fig. 2 and Section 3.2) and possibly nebular emission.

P-Cygni profiles of N V and C IV are best reproduced by a S99 model with a continuous star formation history (SFH) with an age of 9 Myr and $Z_{*}/Z_{\odot} \simeq 0.4$ with a $\chi^2/N_{\text{dof}} = 1.76$ (red in the left bottom panel of Fig. 2), where the number of degree of freedom is $N_{\text{dof}} = 166$. S99 models with $Z_{*}/Z_{\odot} = 0.2$ (and $Z_{*}/Z_{\odot} = 1.0$) overpredict (underpredict) the strength of C IV profile, increasing the χ^2 by a factor $\gtrsim 2.3$. Similarly, S99 models with ages < 4 Myr (and > 20 Myr) will overpredicted (underpredicted) the strength of N V profile. On the other hand, if a burst SFH is assumed, a fairly good fit is found for a burst age of 3–4 Myr, but the fit is still worse ($\chi^2/N_{\text{dof}} = 2.0$) than the one assuming a continuous SFH. Therefore, we consider from now on a continuous SFH with an age of 9 ± 5 Myr and $Z_{*}/Z_{\odot} \simeq 0.4$ as the best fit of J1316+2614. The ionizing production efficiency of this

²<http://www.gtc.iac.es/instruments/osiris/>

³<http://www.gtc.iac.es/instruments/emir/>

⁴<https://pyemir.readthedocs.io/en/latest/index.html>

Table 1. Summary of the GTC spectroscopic observations of J1316+2614.

Instrument	Grism (R)	Spec. range (μm)	Exp. time (s)	Date
OSIRIS	R1000B (700)	0.360–0.750	900×4	2018 April 10
OSIRIS	R2500R (1800)	0.558–0.769	750×12	2021 April 20
EMIR	HK (700)	1.454–2.405	160×16	2018 May 8

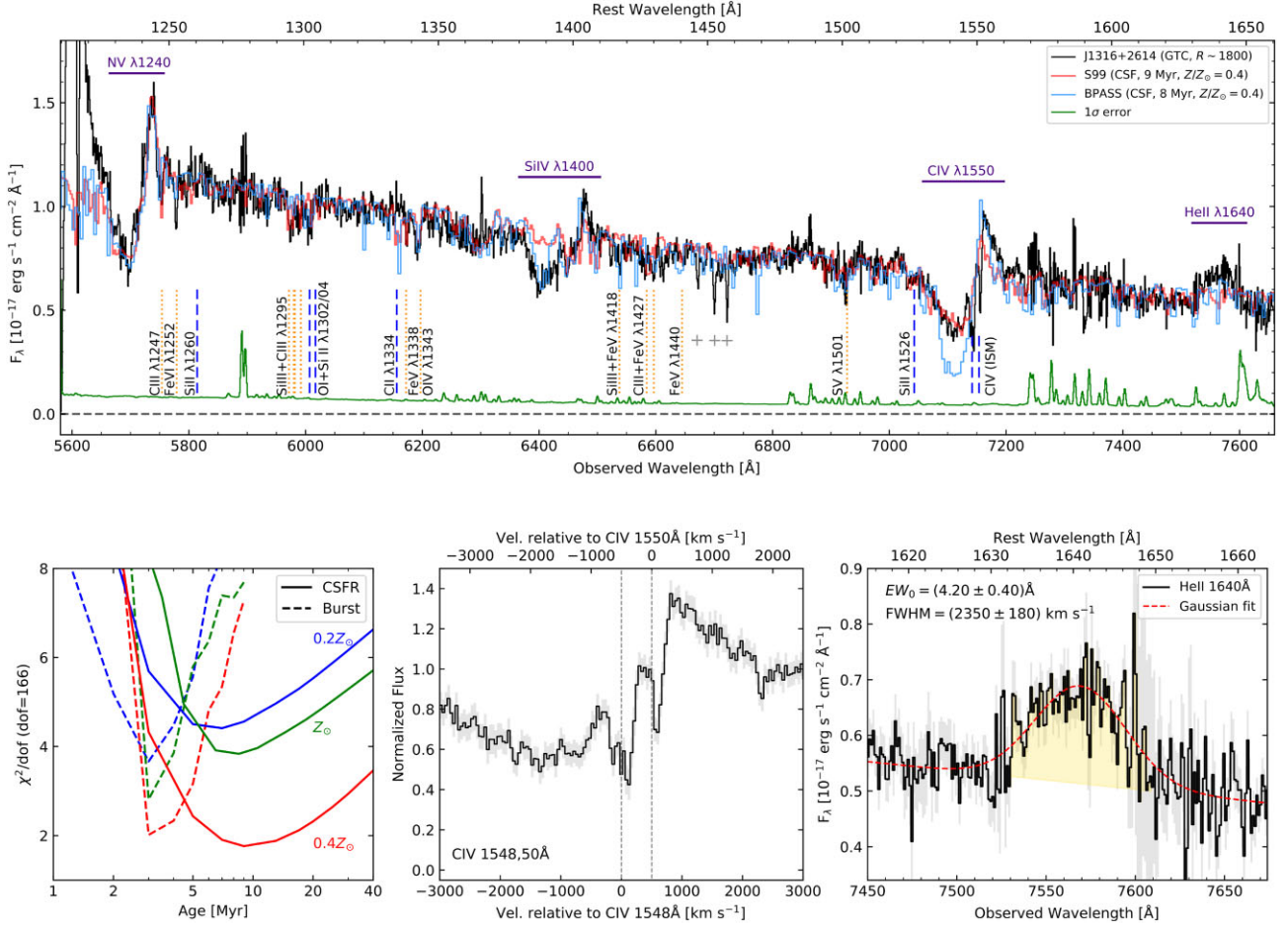


Figure 2. Top panel: GTC/OSIRIS rest-frame UV spectrum of J1316+2614 (black) and its corresponding 1σ uncertainty (green). The vertical lines marked below the spectrum identify the position of low-ionization ISM absorption (blue) and several photospheric absorption lines (yellow), some of them resolved and detected with high significance for which the systemic redshift was derived, $z_{\text{sys}} = 3.6130 \pm 0.0008$. The spectrum also shows three absorption lines that are not related to J1316+2614 (cross symbols), two of them originated from an intervening system at $z \simeq 2.579$ (Al III 1854, 1863 Å). The best-fitting STARBURST99 model with a continuous SFR over an age of 9 Myr and $Z_*/Z_{\odot} = 0.4$ is shown in red. For comparison, a BPASS model with similar stellar properties as the best-fitting STARBURST99 model is also shown (blue). The bottom left-hand panel shows the results of our χ^2 minimization using continuous SFR (solid) and burst (dashed) STARBURST99 models and different metallicities. The bottom middle panel shows a zoom-in into the C IV profile. Two narrow absorption lines associated with the ISM components of C IV (at $\simeq 1548$ and $\simeq 1550$ Å) are detected and are redshifted by $\simeq 100$ km s $^{-1}$ relative to the systemic velocity. The bottom right-hand panel shows the He II emission seen in J1316+2614 (black) and the Gaussian fit (red), with the fitted parameters, EW_0 and FWHM, indicated in the legend.

model, defined as the number of ionizing photons produced per unit UV luminosity ($\xi_{\text{ion}} = Q_{\text{H}}/L_{\text{UV, int}}$), is $\log(\xi_{\text{ion}}[\text{erg}^{-1}\text{Hz}]) = 25.40$. This is higher than the ξ_{ion} inferred for typical high- z Lyman break galaxies (LBGs) ($\log(\xi_{\text{ion}}/\text{erg}^{-1}\text{Hz}) \simeq 24.8$, e.g. Bouwens et al. 2016), but comparable with that inferred for Ly α emitters (LAEs) (e.g. Matthee et al. 2017).

We also take into consideration the dust attenuation. The observed $\beta_{\text{UV}} = -2.59 \pm 0.05$ in J1316+2614 is similar to the intrinsic UV slope inferred for the best-fitting S99 model, $\beta_{\text{UV}}(\text{S99}) = -2.62$, i.e. without considering the effect of dust or the inclusion of nebular

continuum. Therefore, the observed slope is consistent with almost zero attenuation, $E(B - V)_* = 0.006^{+0.018}_{-0.006}$, assuming the Calzetti et al. (2000) extinction curve.

In addition to the NV and CIV P-Cygni profiles, other stellar features are detected and their strengths are relatively well reproduced by the best-fitting S99 model. The photospheric absorption in C III 1247 Å, S V 1501 Å, and some blends from multiple transitions such as S III and C III around ~ 1295 Å and by Fe V and O IV around ~ 1340 Å are well detected (see Fig. 2) and their strengths are consistent with the best-fitting S99 model. As these lines arise from

stellar atmospheres, we use them to determine the systemic redshift of J1316+2614 as $z_{\text{sys}} = 3.6130 \pm 0.0008$.

Lastly, we note the poor agreement of the best-fitting S99 model in two important features, Si IV 1393,1402 Å and He II 1640 Å. A strong P-Cygni contribution is detected in Si IV 1393,1402 Å, but the best-fitting S99 model does not reproduce its strength. Such profiles are usually seen in some early-O type supergiants, Wolf-Rayet (W-R) stars (e.g. Garcia & Bianchi 2004; Crowther et al. 2016) or in metal-rich stars, and might indicate different (lower) effective temperatures. Only S99 models with $Z/Z_{\odot} \geq 1$ can show Si IV profiles with similar strength as the one observed in J1316+2614. However, these high-metallicity models are disfavoured as they predict much stronger absorption in photospheric lines than the observed ones. It is worth to note that BPASS models with similar metallicity as our best-fitting S99 model (i.e. $0.4Z_{\odot}$) can predict relatively well the observed P-Cygni profile in Si IV (shown in blue in Fig. 2 for comparison). The best-fitting S99 model also fails to reproduce the strength of He II 1640 Å emission in J1316+2614 (Fig. 2). Fitting a Gaussian profile to the He II line, we measure a line width $\text{FWHM} = 2350 \pm 180 \text{ km s}^{-1}$ and a rest-frame equivalent width $EW_0 = 4.2 \pm 0.4 \text{ \AA}$. This is much stronger than that found in typical star-forming galaxies ($EW_0^{\text{LBGs}} \simeq 1.3 \text{ \AA}$, e.g. Shapley et al. 2003), and may indicate a significant contribution of stars with mass $> 100 M_{\odot}$ (Senchyna et al. 2021; Martins & Palacios 2022) that show very strong and broad He II emission (e.g. Crowther et al. 2016). A more detailed investigation on the origin of the strong He II in J1316+2614 and in other luminous star-forming galaxies will be presented in a forthcoming work (Upadhyaya et al., in preparation).

3.2 Interstellar medium absorption lines

Interstellar medium (ISM) absorption lines appear very weak in the spectrum of J1316+2614. We checked the presence of the main low-ionization ISM (LIS) lines that are typically observed in many other star-forming galaxies (e.g. Shapley et al. 2003). These include Si II 1260 Å, O I+Si II 1302 Å, C II 1334 Å, or Si II 1526 Å (blue dashed lines in Fig. 2). However, these lines are not detected in the spectrum of J1316+2614 despite the high SNR of the continuum ($\simeq 15\text{--}20 \text{ pix}^{-1}$). We only detect a faint absorption in O I+Si II at the systemic velocity with $EW_0 \simeq 1 \text{ \AA}$, but stellar models can explain its strength (Fig. 2).

On the other hand, two narrow absorption lines are detected at $\simeq 7142$ and $\simeq 7154 \text{ \AA}$ and are consistent to be the ISM components of the C IV doublet (1548 and 1550 Å, see bottom panel of Fig. 2). The lines present narrow profiles being almost unresolved ($\text{FWHM} \lesssim 200 \text{ km s}^{-1}$). They show $EW_0 \simeq 1\text{--}3 \text{ \AA}$, although the uncertainties are large given the difficulty to estimate the continuum level within the P-Cygni profile. Interestingly, the C IV ISM absorption lines are redshifted by $\simeq 100 \text{ km s}^{-1}$ relative to the systemic velocity derived using stellar absorption lines, indicating that the high-ionized ISM is apparently moving towards the young stars.

3.3 Nebular emission

J1316+2614 shows significant ($> 5\sigma$) emission in several nebular lines, such as Ly α 1215 Å, H β 4862 Å, and in the [O III] doublet at 4960 and 5008 Å. These are shown in Fig. 3.

The Ly α line shows two peaks around the systemic velocity, with the blue peak more intense than the red one. We measure a ratio between the blue and red emission $I_B/I_R = 3.7 \pm 0.1$ and a velocity peak separation $\Delta v(\text{Ly}\alpha) = 680 \pm 70 \text{ km s}^{-1}$. Fitting a Gaussian profile to the blue and red emission, we find line widths

of 440 and 510 km s^{-1} (FWHM, and corrected for instrumental broadening), respectively. We note, however, that these lines do not show a symmetric profile and therefore are not well reproduced by Gaussian profiles. Because the continuum level around Ly α is not easy to constrain (due to the IGM absorption and the N V 1240 Å P-Cygni profile at shorter and longer wavelengths, respectively), we subtract and divide our spectrum by the best-fitting S99 model. We then measure the flux and equivalent width of the nebular component of Ly α by integrating its flux within the spectral region $\pm 1000 \text{ km s}^{-1}$ around the systemic velocity. Ly α has a total flux of $F(\text{Ly}\alpha) = (9.62 \pm 0.02) \times 10^{-16} \text{ erg s}^{-1} \text{ cm}^{-2}$, and $EW_0 = 20.5 \pm 1.9 \text{ \AA}$, corresponding to a luminosity $\log_{10}(L_{\text{Ly}\alpha}/\text{erg s}^{-1}) = 44.09 \pm 0.10$. These values are consistent with those measured using the BOSS spectrum, which uses a larger aperture (2 arcsec-diameter fiber) than OSIRIS (1 arcsec-width), suggesting that there is little scatter at larger radii.

It is worth to note that Ly α profiles like this, i.e. showing the blue peak more intense than the red one, are extremely rare. It has been observed only in a few star-forming galaxies (Wofford, Leitherer & Salzer 2013; Erb et al. 2014; Trainor et al. 2015; Izotov et al. 2020; Furtak et al. 2022) and in other type of sources, such as AGNs or extended Ly α nebulae (Martin et al. 2015; Vanzella et al. 2017; Ao et al. 2020; Daddi et al. 2021; Li et al. 2022). This profile is usually linked to radial infall of gas (Dijkstra, Haiman & Spaans 2006). Other scenarios, such as emission from two kinetically different sources (e.g. merger) or disc rotation, are unlikely. In such cases, similar doubled-peaked profiles should be present in other nebular lines, which is not the case. As described next, rest-frame optical lines in J1316+2614 do not show this complex profile and can be well modelled with single Gaussian profiles. We note however that rest-frame optical lines are observed with much lower spectral resolution and SNR than Ly α , which makes it difficult a direct comparison of their profiles.

Turning to the rest-frame optical lines, three Gaussian profiles are used to fit simultaneously H β and [O III] 4960,5008 Å, and a constant (in f_{λ}) for the continuum. We measure $F(\text{H}\beta) = (9.1 \pm 1.4) \times 10^{-17} \text{ erg s}^{-1} \text{ cm}^{-2}$, $F([\text{OIII}] 4960) = (15.5 \pm 2.2) \times 10^{-17} \text{ erg s}^{-1} \text{ cm}^{-2}$, and $F([\text{OIII}] 5008) = (42.5 \pm 3.8) \times 10^{-17} \text{ erg s}^{-1} \text{ cm}^{-2}$. The lines appear barely resolved only, with $\text{FWHM} \sim 380 \text{ km s}^{-1}$ after correcting for the EMIR instrumental broadening ($\simeq 450 \text{ km s}^{-1}$). The continuum in the K band is detected with a flux density corresponding to $m(K) = 21.42 \pm 0.13$ mag. We find rest-frame equivalent widths for H β and [O III] 4960 Å and [O III] 5008 Å of 34.7 ± 6.8 , 59.3 ± 10.8 , and $162.0 \pm 23.9 \text{ \AA}$, respectively. Emission in nebular [O II] 3727,3729 Å is also detected around $\lambda \simeq 1.72 \text{ \mu m}$, but with low significance ($\simeq 2.5\sigma$) with a flux of $F([\text{OII}]) = (8.9 \pm 3.6) \times 10^{-17} \text{ erg s}^{-1} \text{ cm}^{-2}$. Table 2 summarizes our measurements.

Assuming case B recombination and $T = 10^4 \text{ K}$, the intrinsic ratio between Ly α and H β is 24.8. Using the observed fluxes of Ly α and H β and considering $E(B - V) = 0$, we infer a Ly α escape fraction $f_{\text{esc}}(\text{Ly}\alpha) = 0.43 \pm 0.12$. We measure the line ratio $R23 = ([\text{O II}] + [\text{O III}])/H\beta = 7.1 \pm 1.8$, for which we measure a nebular abundance $12 + \log(\text{O}/\text{H}) = 8.45 \pm 0.12$ ($\simeq 0.5Z_{\odot}$) following Pilyugin & Thuan (2005). This is compatible with the stellar metallicity inferred for the young stellar population. A line ratio $[\text{O III}]/[\text{O II}]$ of $O_{32} = 4.8 \pm 2.1$ is also inferred and will be discussed in more detail in Section 4.2.5. Note that, as discussed in Section 4.2, the high LyC escape fraction in J1316+2614 (Section 3.5) is reducing the observed intensity of the nebular emission, and the suppression factor might be different for recombination (Ly α , H β) and forbidden metal lines ([O II], [O III]). This means that the nebular abundance

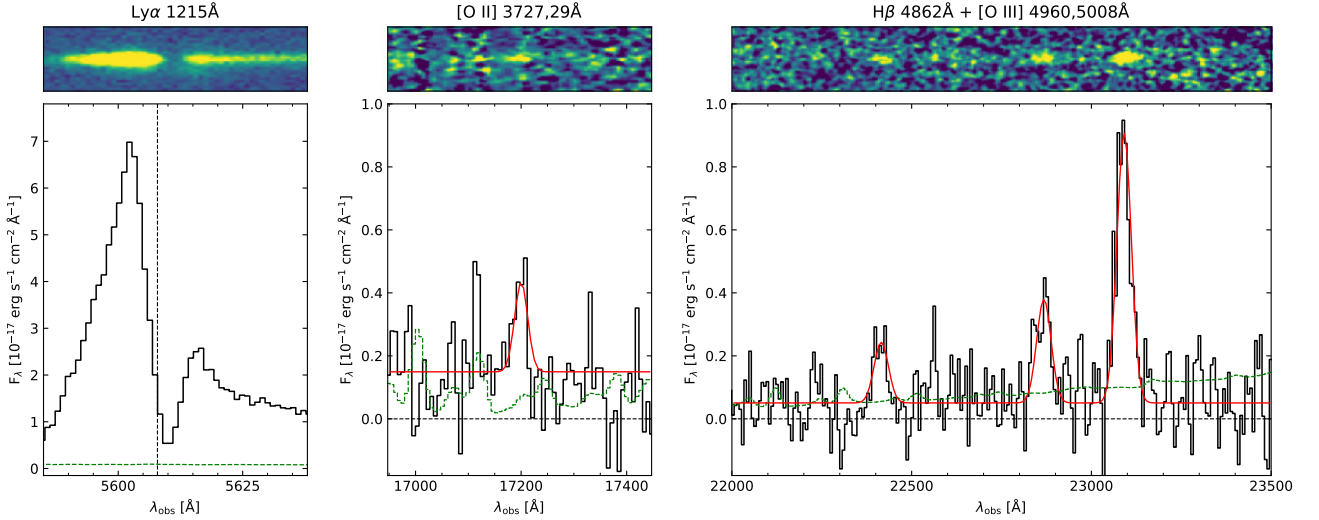


Figure 3. Nebular emission detected in J1316+2614. The left-hand panel shows the Ly α emission (black and 1σ error in green) seen in the medium resolution OSIRIS spectrum. It shows a double-peaked emission around the systemic velocity (vertical dashed line). The blue peak is more intense than the red one, suggestive of neutral gas infall. The middle and right-hand panels show the near-IR spectrum with EMIR around the regions of [O II] and H β + [O III], respectively. 1σ error is shown in green and the performed Gaussian fits for each line are shown in red.

Table 2. Nebular emission in J1316+2614.

Line	EW_0 [\AA]	Flux [$10^{-17} \text{ erg s}^{-1} \text{ cm}^{-2}$]
Ly α 1215 \AA	20.5 ± 1.9	96.2 ± 2
[O II] 3727,3729 \AA	12.9 ± 5.0	8.9 ± 3.6
H β 4862 \AA	34.7 ± 6.8	9.1 ± 1.4
[O III] 4960 \AA	59.3 ± 10.8	15.5 ± 2.2
[O III] 5008 \AA	162.0 ± 23.9	42.5 ± 3.8

inferred using $R23$ might not be valid and should be treated with caution.

3.4 LyC emission

The 40 min low-resolution spectrum of J1316+2614 is shown in Fig. 4 and presents significant emission below $\lambda_{\text{obs}} \simeq 4200 \text{ \AA}$, i.e. $\lambda_0 < 911.8 \text{ \AA}$, which can be associated with LyC leakage. The emission is clearly detected down to rest-frame wavelengths $\simeq 830 \text{ \AA}$ (rest) with a total SNR $\simeq 17$ from 830 to 910 \AA and an average SNR per spectral bin of $\simeq 1.6 \text{ pix}^{-1}$. We measure a flux density in the spectral region between 830 and 910 \AA (rest) of $f_{870}(\text{obs}) = 1.69 \pm 0.10 \mu\text{Jy}$, corresponding to a magnitude of $m_{870} = 23.33 \pm 0.06$ (AB). This yields a ratio of the ionizing to non-ionizing flux density $(f_{870}/f_{1500})_{\text{obs}} = 0.146 \pm 0.011$ or $\Delta m = 2.1$ (AB).

The relative LyC photon escape fraction along the line of sight, $f_{\text{esc,rel}}(\text{LyC})$, is inferred by comparing the observed ratio of the ionizing to non-ionizing flux density of J1316+2614, $(f_{870}/f_{1500})_{\text{obs}}$, to that from the best-fitting S99 model derived in Section 3.1, $(f_{870}/f_{1500})^{\text{S99}}$, using the following formulation:

$$f_{\text{esc,rel}}(\text{LyC}) = \frac{(f_{870}/f_{1500})_{\text{obs}}}{(f_{870}/f_{1500})^{\text{S99}}} \times \frac{1}{T(\text{IGM})}, \quad (1)$$

where $T(\text{IGM})$ is the IGM transmission, and flux ratios refer to f_{ν} . Using the same rest-frame spectral windows of 830–910 and 1490–1510 \AA , we infer $(f_{870}/f_{1500})^{\text{S99}} = 0.27$. This means that $f_{\text{esc,rel}}(\text{LyC}) = 0.54/T(\text{IGM})$, which implies that $T(\text{IGM})$ should be at least larger than >0.54 to keep a physical $f_{\text{esc,rel}}(\text{LyC}) \leq 1$ (e.g. Vanzella et al.

2012). This also implies that $f_{\text{esc,rel}}(\text{LyC})$ must be ≥ 0.54 , where the most extreme value (0.54) stands for a completely transparent IGM ($T(\text{IGM}) = 1.0$).

A precise estimate of $T(\text{IGM})$ below $<912 \text{ \AA}$ (thus $f_{\text{esc}}(\text{LyC})$) is not possible due to the stochastic nature and large fluctuation of the attenuation in one single line of sight (e.g. Inoue & Iwata 2008; Inoue et al. 2014). To overcome this, we infer $T(\text{IGM})$ in the non-ionizing part of the spectrum of J1316+2614, from 912 to 1215 \AA , and assume that it is similar at $\lambda_0 < 912 \text{ \AA}$. Following Marques-Chaves et al. (2021), we compare the flux of J1316+2614 to that of the best-fitting S99 model in several spectral regions from 912–1215 \AA (marked in Fig. 4 as grey horizontal bars), probing only H I absorbers from the Lyman forest. By doing this, we are excluding spectral regions associated with the Lyman series, ISM and circumgalactic medium (CGM) from J1316+2614, which are not included in S99 models. We derive a mean value and standard deviation $T(\text{IGM}) = 0.59 \pm 0.17$, and assume this values for $\lambda_0 < 912 \text{ \AA}$. The inferred $T(\text{IGM})$ in J1316+2614 is significantly larger than those obtained by other works using Monte Carlo simulations of the IGM transmission ($\langle T(\text{IGM}) \rangle \simeq 0.2$ at $z \sim 3.5$, e.g. Steidel et al. 2018). This suggests that the large flux density observed in J1316+2614, $f_{870}(\text{obs})$, is due to the combination of a large $f_{\text{esc,rel}}(\text{LyC})$ and a favourable IGM transmission. In Section 4.3, we discuss the implications of a favourable IGM transmission and other uncertainties regarding the adopted stellar model.

Using equation (1) we infer $f_{\text{esc,rel}}(\text{LyC}) \sim 0.92_{-0.20}^{+0.08}$. We note that this value refers to the LyC escape fraction measured between 830–910 \AA and along the line of sight. The uncertainties on $f_{\text{esc,rel}}(\text{LyC})$ refer to those arising from $T(\text{IGM})$. Other sources of uncertainty should be less relevant or they are difficult to quantify. For example, the properties of the young stellar population, namely the age and metallicity, are relatively well constrained from the modelling of the stellar wind profiles (see Section 3.1). Their uncertainties should not impact significantly on the inferred $f_{\text{esc,rel}}(\text{LyC})$ (see more discussion in Section 4.3), but we also note they are model dependent. On the observational side, uncertainties due to the flux calibration or differential slit-losses between $\lambda_0 < 912 \text{ \AA}$ and $\lambda_0 \simeq 1500 \text{ \AA}$ are difficult to constrain. Nevertheless, the low-resolution GTC spectrum

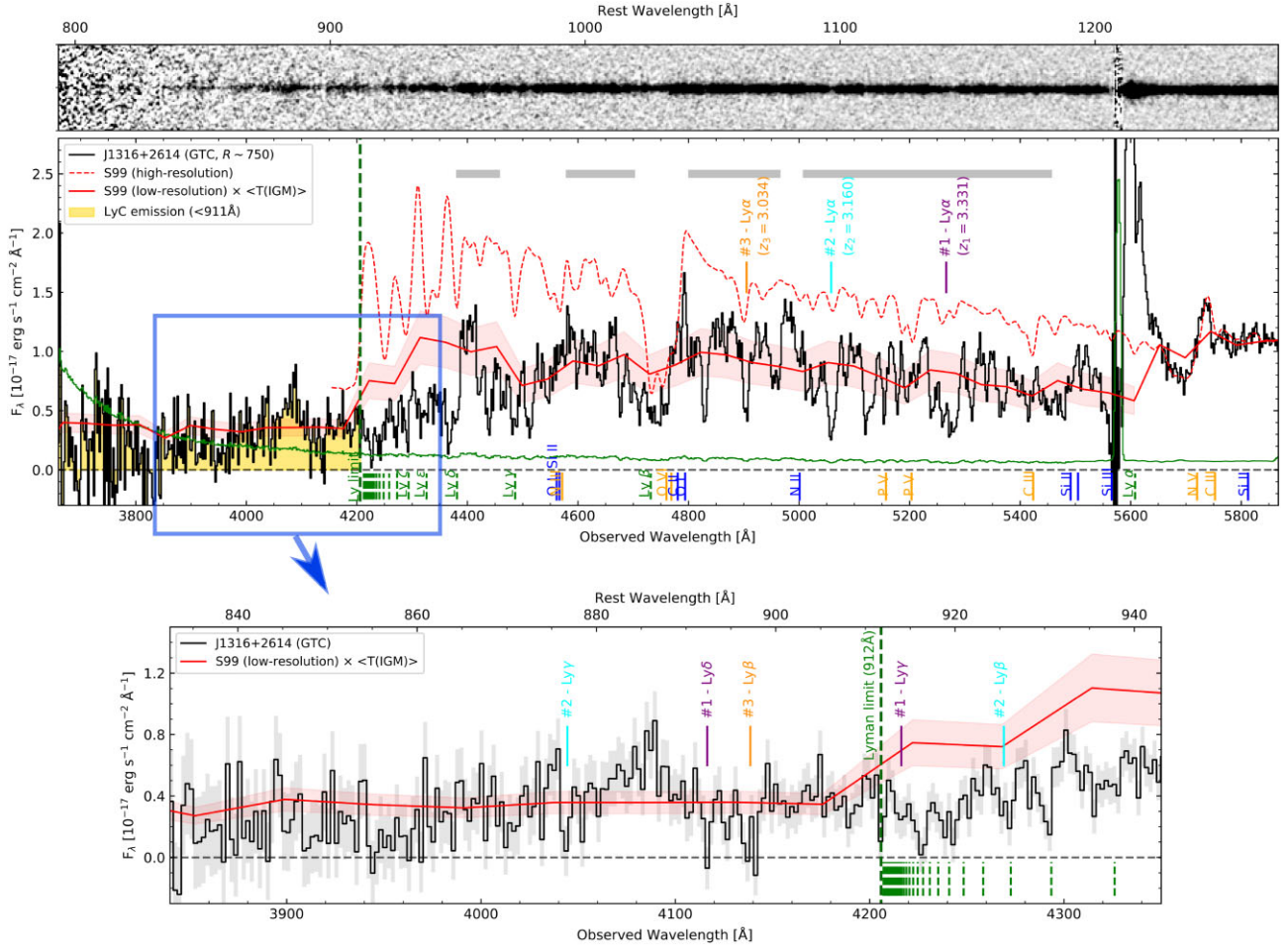


Figure 4. 2D and 1D GTC low-resolution spectrum of J1316+2614 (black) and 1σ uncertainty (green). The spectral region in yellow corresponds to the emission below $\lambda_0 < 912 \text{ \AA}$, which is related to LyC emission. The position of the Lyman limit is marked with a green dashed line. The high- and low-resolution best-fitting S99 models (9 Mry age, $Z_*/Z_\odot = 0.4$ and $E(B - V)_* = 0.0$) are shown in dashed and solid red, respectively. The latter is corrected for the IGM transmission ($\langle T(IGM) \rangle = 0.59 \pm 0.17$). The horizontal grey lines mark the spectral windows used to infer $T(IGM)$, probe H I absorbers from the Lyman forest in the line of sight only and excluding other regions associated with the Lyman series and ISM from J1316+2614 (marked as green and blue vertical lines, respectively, below the 1d spectrum). The vertical yellow lines mark the position of stellar features associated with J1316+2614. The vertical lines above the spectrum mark the position of three strong H I absorbing systems identified at $z = 3.331, 3.160,$ and 3.034 (#1 to #3, respectively). The bottom panel shows a zoom-in to the LyC region.

matches very well to that of BOSS spectrum, where LyC is also detected.

Assuming $E(B - V) = 0.006$, the absolute LyC escape fraction is $f_{\text{esc,abs}}(\text{LyC}) = 0.87^{+0.08}_{-0.20}$. Given this, we estimate the number of ionizing photons escaping from J1316+2614, Q_H^{esc} , by

$$Q_H^{\text{esc}} = f_{\text{esc,abs}}(\text{LyC}) \times Q_H^{\text{int}}, \quad (2)$$

where $Q_H^{\text{int}} = (8.5 \pm 1.7) \times 10^{55} \text{ s}^{-1}$ is the intrinsic ionizing photon production rate from the best-fitting S99 model scaled to the absolute magnitude $M_{\text{UV}} = -24.7$ of J1316+2614. We infer $Q_H^{\text{esc}} = (7.3 \pm 2.0) \times 10^{55} \text{ s}^{-1}$.

3.5 Multiwavelength SED

In this section, we perform analysis of the multiwavelength photometry and SED of J1316+2614. Optical photometry in $g, r, i,$ and z bands are retrieved from SDSS using the MODEL photometry. For the near-IR images ($Y, J, H,$ and K_s) we use aperture photometry with a diameter of $2.5 \times \text{FWHM}$. J1316+2614 is not resolved in

the optical (SDSS) or near-IR (EMIR/GTC) with seeing conditions $\simeq 0.9\text{--}1.2$ arcsec FWHM. J1316+2614 is not detected in the mid-IR in the WISE2020 Catalog (Marocco et al. 2021) at 3.4 \mu m (W1) and 4.6 \mu m (W2), with $W1 > 21.45$ and $W2 > 20.84$ at 5σ . Table 3 summarizes the optical to mid-IR photometry of J1316+2614.

Fig. 5 (left) shows the inferred photometry of J1316+2614. It shows a blue SED with optical to mid-IR colour $r - W1 < -0.3$. This is much bluer than the typical colours measured in type-I/II AGNs at similar redshift, $r - W1 \simeq 0.6$ (Selsing et al. 2016; Pâris et al. 2018). This is another evidence of the lack of a strong/dominant AGN component in J1316+2614.

To investigate the SED properties of J1316+2614, we perform SED-fitting with CIGALE code (Burgarella et al. 2005; Boquien et al. 2019) using the available photometry covering a rest-frame wavelength $0.1\text{--}1.0 \text{ \mu m}$. The fit also includes flux measurements of the $\text{H}\beta + [\text{O III}]$ emission lines (Table 3). We assume an SFH with two components, a young stellar component with a continuous SFR with age ≤ 20 Myr (see Section 3.1), and an exponentially declining SFH with age of ≥ 200 Myr to probe the old stellar population.

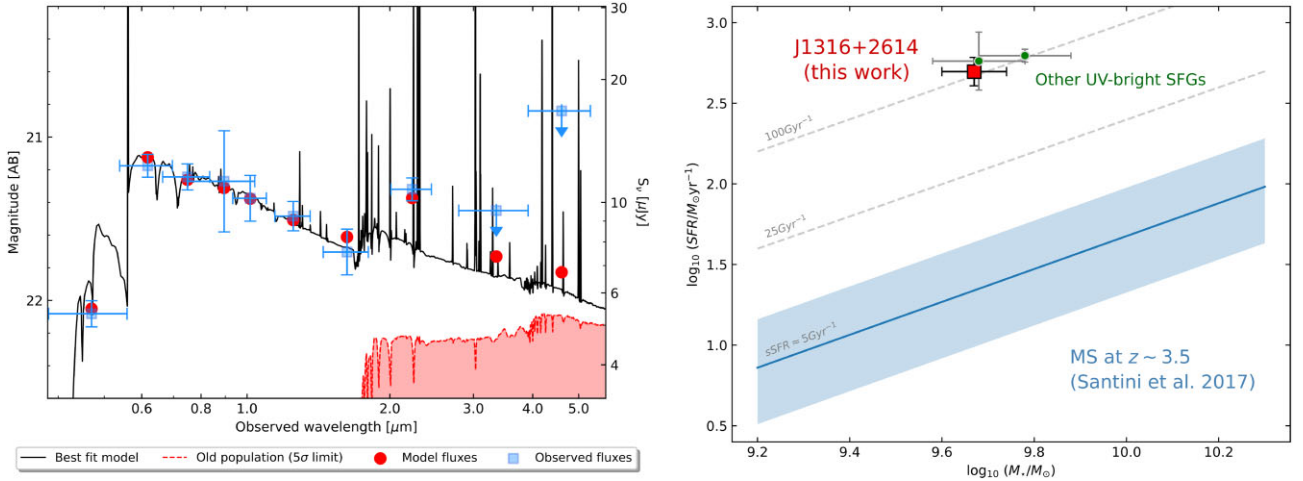


Figure 5. Left-hand panel: SED best-fitting model (black) of J1316+2614 using CIGALE (Burgarella, Buat & Iglesias-Páramo 2005). The fit uses photometry from g to WISE $W2$ (blue squares, see Table 3), covering the rest-frame wavelength 0.1–1.0 μm . The predicted fluxes from the best fit in each band are marked with red circles. The SED of J1316+2614 is dominated by a young stellar population with an age 14 ± 4 Myr and a continuous star formation rate $\text{SFR} = 496 \pm 92 M_{\odot} \text{yr}^{-1}$. The young stellar population has a stellar mass $\log(M_{*}/M_{\odot}) = 9.67 \pm 0.07$ with a dust attenuation $E(B - V) = 0.035 \pm 0.016$. The old stellar population is not well constrained and we infer a 5σ limit for the stellar mass $\log(M_{*}/M_{\odot}) \leq 10.3$ for a 580 Myr age (red shaded region). Right-hand panel: Relation between SFR and stellar mass of J1316+2614 (red square) and the other few star-forming galaxies known brighter than $M_{\text{UV}} < -24$ (green circles, from Marques-Chaves et al. 2020b and Marques-Chaves et al. 2021, and assuming a Chabrier 2003 IMF). The solid blue line and region mark, respectively, the observed main-sequence and scatter of star-forming galaxies at $z \simeq 3.5$ of Santini et al. (2017).

Table 3. Optical to mid-IR photometry of J1316+2614.

Band	λ_{eff} (μm)	Magnitude (AB)	Telescope
g	0.47	22.08 ± 0.08	SDSS
r	0.61	21.18 ± 0.05	SDSS
i	0.77	21.24 ± 0.08	SDSS
z	0.89	21.27 ± 0.31	SDSS
Y	1.01	21.38 ± 0.14	EMIR/GTC
J	1.25	21.48 ± 0.09	EMIR/GTC
H	1.61	21.70 ± 0.14	EMIR/GTC
K_s	2.14	21.31 ± 0.07	EMIR/GTC
$W1$	3.35	>21.45 (5σ)	WISE
$W2$	4.60	>20.84 (5σ)	WISE

Stellar population models from Bruzual & Charlot (2003), Chabrier (2003) IMF, and the Calzetti et al. (2000) dust attenuation law are considered. We fix the metallicity $Z/Z_{\odot} = 0.4$ based on our analysis in Section 3.1, and the escape of ionizing photons is set as a free parameter (i.e. 0.0–1.0).

The best-fitting model obtained for J1316+2614 is shown in the left-hand panel of Fig. 5 (black). The young stellar population is characterized by an age of 14 ± 4 Myr and $\text{SFR} = 496 \pm 92 M_{\odot} \text{yr}^{-1}$, consistent with the far-UV analysis in Section 3.1. We infer a burst mass $\log(M_{*}/M_{\odot}) = 9.67 \pm 0.07$ and dust attenuation $E(B - V) = 0.035 \pm 0.016$. The LyC escape fraction is $f_{\text{esc}}(\text{LyC}) = 0.65 \pm 0.09$. On the other hand, the mass of the old stellar population (age 580 ± 285 Myr) is not well constrained and we provide a 5σ limit of $\log(M_{*}/M_{\odot}) \leq 10.3$ (in red in Fig. 5, left). The SED properties derived from the multiwavelength photometry agree well with those inferred from the UV fitting.

Our results indicate that the rest-frame UV to near-IR SED of J1316+2614 is dominated by the young stellar population, and if an old stellar population is present it should be less massive than $\log(M_{*}/M_{\odot}) \leq 10.3$ (5σ). Considering the stellar mass of the young stellar population, we infer a high specific SFR ($\text{sSFR} = \text{SFR}/M_{*}$) of

$105 \pm 49 \text{Gyr}^{-1}$. The right-hand panel of Fig. 5 shows the position of J1316+2614 in the SFR versus M_{*} diagram and a comparison with main-sequence (MS) star-forming galaxies at similar redshifts (Santini et al. 2017). J1316+2614 is offset of the MS by 1.5 dex. The other few star-forming galaxies known brighter than $M_{\text{UV}} < -24$ at $z \sim 3$ also show similar sSFR $\sim 100 \text{Gyr}^{-1}$ (green in Fig. 5, Marques-Chaves et al. 2020b, 2021). Even considering the mass of the old stellar population, J1316+2614 ($M_{*}^{\text{total}}/M_{\odot} \leq 10.6$) will be still located above the MS by $\simeq 0.7$ dex.

4 DISCUSSION

J1316+2614 is one of the most luminous star-forming galaxies in the UV and Ly α discovered so far, with $M_{\text{UV}} = -24.68 \pm 0.08$ and $\log_{10}(\text{Ly}\alpha / \text{erg s}^{-1}) = 44.08 \pm 0.10$, and in addition, one of the strongest LyC emitters known. In this section, we discuss its properties, compare with those of other strong LyC emitters, and discuss the implications of such discovery. Table 4 summarizes the main properties of J1316+2614.

4.1 AGN contamination or low- z interloper?

We start investigating the possible contribution of an AGN or a low-redshift contaminant to the flux detected below $\lambda_0 < 912 \text{\AA}$.

The rest-frame UV spectrum of J1316+2614 shows a wealth of absorption lines that originated in the photospheres of hot stars. Fig. 6 shows a zoom-in of the GTC spectrum around $\lambda_0 \simeq 1300$ – 1400\AA and $\lambda_0 \simeq 1500 \text{\AA}$, where some of these lines are clearly detected. The detection of these intrinsically weak photospheric lines indicates that the UV continuum of J1316+2614 is dominated by stellar emission, rather than an AGN, otherwise these absorption lines would be washed-out. For illustration, Fig. 6 also shows the spectrum of a O8.5 Iaf-type star from the Large Magellanic Cloud observed with *HST*/STIS (LH 9-34, obtained as part of the ULLYSES program Roman-Duval et al. 2020). In addition, we also show the composite

Table 4. Summary of the properties of J1316+2614.

	Value	Uncertainty
RA (J2000)	13:16:29.61	0.1 arcsec
Dec. (J2000)	+26:14:07.05	0.1 arcsec
z_{sys}	3.6130	0.0008
M_{UV} (AB)	-24.68	0.08
β_{UV}	-2.59	0.05
$\log(L[\text{Ly } \alpha/\text{erg s}^{-1}])$	44.09	0.10
$\log(L[\text{H } \beta/\text{erg s}^{-1}])$	43.18	0.10
$EW_0(\text{Ly } \alpha)$ (Å)	20.5	1.9
$EW_0(\text{H } \beta)$ (Å)	34.7	6.8
Z_*/Z_{\odot}	0.4	[0.2–1.0]
$12 + \log(\text{O}/\text{H})$	8.45	0.12
Age (Myr) [young]	9 – 14 ^a	[5–20] ^a
$\log(M_*/M_{\odot})$ [young]	9.67	0.07
$\log(M_*/M_{\odot})$ [old]	≤ 10.3	–
$E(B - V)$	0.006 – 0.034 ^a	[0–0.05] ^a
SFR ($M_{\odot} \text{ yr}^{-1}$)	497	92
sSFR (Gyr^{-1})	105	49
ΣSFR ($M_{\odot} \text{ yr}^{-1} \text{ kpc}^{-2}$)	≥ 10	–
$\log(\xi_{\text{ion}}[\text{Hz erg}^{-1}])$	25.40	0.10
$f_{\text{esc}}(\text{Ly } \alpha)$	0.43	0.12
$f_{\text{esc, rel}}(\text{LyC})$	0.92	[-0.20, +0.08]
$f_{\text{esc, abs}}(\text{LyC})$	0.87	[-0.20, +0.08]
$\log(Q_H^{\text{esc}}/\text{s}^{-1})$	55.86	0.11

Note. ^aAge of the young stellar population and dust attenuation obtained with different methods: using UV spectral features and from the best-fitting model of the SED using CIGALE, respectively.

spectrum of bright QSOs of Selsing et al. (2016) obtained with X-Shooter. As clearly seen in the figure, photospheric lines (highlighted in yellow) are detected both in the spectra of J1316+2614 and the LH 9-34 star, but are not present in the spectra of QSOs.

Other spectral features, such as the P-Cygni profiles in wind lines of N V 1240 Å and C IV 1550 Å, can be well explained by a young stellar population (Section 3.1), which is consistent with the multiwavelength SED (Section 3.5). J1316+2614 shows a blue colour between UV and near-IR (rest-frame) of $r - W1 < -0.3$, which is difficult to explain by a type-I/II AGN component. AGNs show typically much redder colours ($r - W1 \simeq 0.6$ Pâris et al. 2018) than the observed ones. J1316+2614 also shows a very blue UV slope $\beta_{\text{UV}} = -2.60$, much steeper than those commonly observed in QSOs ($\simeq -1.0$ to $\simeq -1.7$, Lusso et al. 2015; Selsing et al. 2016; Liu et al. 2022, but see Lin et al. 2022). Lastly, the nebular emission in J1316+2614 presents narrow profiles without any hint for a broad component ($\text{FWHM} > 1000 \text{ km s}^{-1}$).

Our results clearly indicate that the large luminosity of J1316+2614 is being powered by massive star formation. These do not discard the presence of a low-luminosity AGN (e.g. Seyfert 2 or LINER), but rather indicate that a possible contribution of an AGN to the UV emission should be minimal. The same should be applied to the LyC emission. To quantify this, we consider conservatively a significant contribution of an AGN to the UV continuum of J1316+2614 of ~ 25 per cent, which is compatible with an AGN with an absolute magnitude $M_{\text{UV}}^{\text{AGN}} \simeq -23.2$. Assuming that the observed LyC flux arises from the AGN, this yields $(f_{\text{LyC}}/f_{1500})_{\text{AGN}}^{\text{obs}} \simeq 0.60$. AGNs with LyC detection at similar redshift and luminosities show much lower values $((f_{\text{LyC}}/f_{1500})_{\text{AGN}} \simeq 0.05\text{--}0.25$; Lusso et al. 2015; Cristiani et al. 2016; Micheva, Iwata & Inoue 2017), even noting that the $f_{\text{esc}}(\text{LyC})$ in these AGNs can be as high as 100 per cent. Therefore, a large contribution of an AGN to the LyC emission of J1316+2614 is highly unlikely.

Another source of contamination to the observed LyC emission could arise from a low- z interloper. J1316+2614 appears unresolved in optical and near-IR images, but the poor spatial resolution from these observations ($\simeq 0.9\text{--}1.2$ arcsec FWHM) prevents us to rule out the presence of a low- z interloper close to J1316+2614. From the low-resolution 2D spectrum, the spatial profiles of the emission observed below and above the Lyman edge at $\lambda_{\text{obs}} \simeq 4200 \text{ \AA}$ (i.e. $\lambda_{\text{rest}} \simeq 912 \text{ \AA}$) are similar, both unresolved and co-spatial. This means that if a low- z interloper is present, it should be co-spatial with J1316+2614.

Considering the presence of a contaminant source at $z \gtrsim 0.5$, the emission seen $\lambda_{\text{obs}} < 4200 \text{ \AA}$ would correspond to rest-frame UV radiation and therefore strong emission would be expected from the main rest-frame optical lines (e.g. [O II], [O III], H β , or H α). However, we do not detect any other emission line within the spectral range covered by our optical and near-IR spectra (0.36 to 1.00 μm with GTC/OSIRIS and SDSS, and 1.45 to 2.41 μm with GTC/EMIR), rather than those originated from J1316+2614 at $z = 3.613$. A high-redshift contaminant ($z \gtrsim 2$) is also unlikely, because the flux density measured below $\lambda_{\text{obs}} \lesssim 4200 \text{ \AA}$ is already very large ($\simeq 1.70 \mu\text{Jy}$ or $m \simeq 23.3$ AB). LBGs or LAEs at $z \geq 2$ are much fainter in the UV with typical apparent magnitudes at λ_{rest} of ($m_{\text{UV}} \simeq 24.5\text{--}25.5$, e.g. Reddy & Steidel 2009). Finally, the GTC spectrum of J1316+2614 shows absorption features in the LyC spectral range, which are consistent with Lyman series at redshifts between $z \simeq 3.034$ and $z \simeq 3.331$ (systems #1, #2, and #3 in Fig. 4). This suggests that the emission observed at $\lambda_{\text{obs}} < 4200 \text{ \AA}$ arises from the LyC emission of J1316+2614.

4.2 Intrinsically high LyC leakage from indirect tracers

In the previous section, we shown that an AGN or a lower z interloper should not contribute significantly to the flux observed below $\simeq 4200 \text{ \AA}$ (i.e. the Lyman limit at $z = 3.613$). Here, we discuss the evidence towards a high LyC leakage in J1316+2614 using indirect methods (summarized in Table 5).

4.2.1 Weak nebular lines and continuum emission: β_{UV} and $EW_0(\text{H}\beta)$ plane

One evidence for high leakage is the *weak* nebular lines and continuum emission in J1316+2614. For a young stellar population of $\simeq 9\text{--}14$ Myr old, strong nebular emission would be expected. Assuming a 9 Myr stellar population with a continuous SFH, an IMF with an upper mass limit of $100M_{\odot}$, and $Z = 0.4Z_{\odot}$, the models predict equivalent widths in the Ly α and H β recombination lines of $EW_0(\text{Ly}\alpha) \simeq 120 \text{ \AA}$ and $EW_0(\text{H}\beta) \simeq 145 \text{ \AA}$, respectively (Schaerer & de Barros 2009). The predicted EW_0 s are a factor of $\simeq 4\text{--}6\times$ larger than the ones observed in J1316+2614 (Table 2). The weak nebular emission also affects the SED of J1316+2614 (Fig. 5), making the observed fluxes in the K_s and WISE 3.6 μm bands much weaker than expected if $f_{\text{esc}} = 0$, due to the contribution of H β + [O III] and H α , respectively. In addition, the $\beta_{\text{UV}} = -2.59 \pm 0.05$ measured in spectrum of J1316+2614 is similar to the intrinsic (best fit) S99 stellar model, $\beta_{\text{UV}}(\text{S99}) = -2.62$, i.e. without considering the inclusion of nebular continuum or dust attenuation. This clearly suggests that the contribution of the nebular continuum and dust attenuation should be residual in J1316+2614.

Since the escape of ionizing photons into the IGM/CGM should not contribute to photoionization in the ISM, a large LyC leakage would explain the weak nebular contributions in J1316+2614.

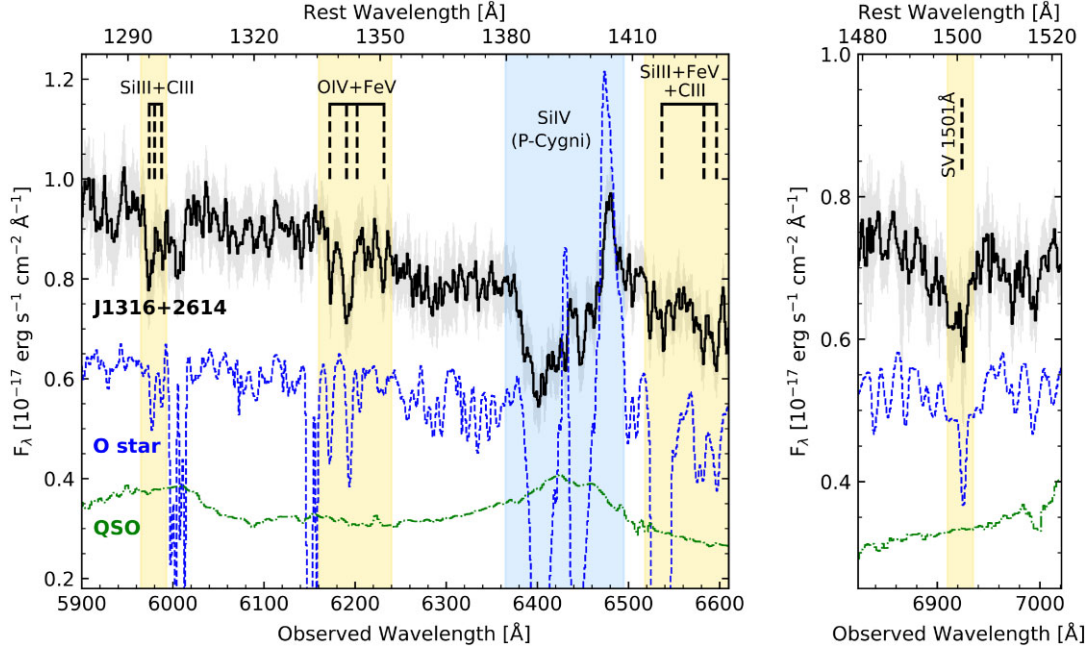


Figure 6. Zoom-in of the GTC spectrum (black, smoothed for visual propose) around $\lambda_0 \simeq 1300\text{--}1400 \text{ \AA}$ (left) and $\lambda_0 \simeq 1500 \text{ \AA}$ (right), where several photospheric lines and a P-Cygni profile in Si IV are detected (highlighted in yellow and blue shaded regions). For comparison, the *HST*/STIS spectrum of a O8.5 Iaf-type star from the Large Magellanic Cloud (LH 9-34, Roman-Duval et al. 2020) and the XShooter composite spectrum of bright QSOs (Selsing et al. 2016) are also shown in blue and green, respectively.

Table 5. Direct and indirect LyC measurements of J1316+2614.

Method	$f_{\text{esc, abs}}(\text{LyC})$	σ	Section
Direct LyC obs.	0.87	$[-0.20, +0.08]$	3.4
Multi-wav. SED	0.65	± 0.09	3.5
β_{UV} versus $EW_0(H\beta)$	≈ 0.8	> 0.5	4.2.1
$L(H\beta)$	0.82	± 0.1	4.2.2
ISM abs. lines	> 0.65	3σ	4.2.3
$\Delta v(\text{Ly}\alpha)$	0	–	4.2.4

To demonstrate this, Fig. 7 shows the relation between β_{UV} and $EW_0(H\beta)$ as a function of $f_{\text{esc}}(\text{LyC})$ following the predictions of Zackrisson et al. (2013) and Zackrisson et al. (2017). For this, we assume S99 models with a continuous SFH with ages between 1 and 50 Myr, and a metallicity $Z = 0.4Z_{\odot}$. For $H\beta$, we use the models of Schaerer & de Barros (2009) matched to the same stellar properties. Nebular continuum and emission are reduced by a factor of $(1 - f_{\text{esc}}(\text{LyC}))$. No dust attenuation is considered, since this effect is expected to be residual in J1316+2614. As seen in this figure, the observed β_{UV} and $EW_0(H\beta)$ in J1316+2614 (red square) is well explained by an $f_{\text{esc}}(\text{LyC}) \simeq 0.8$ at the age of 9 Myr. The figure also shows that $f_{\text{esc}}(\text{LyC}) \leq 0.5$ can be ruled out. This is compatible with the $f_{\text{esc}}(\text{LyC}) \simeq 0.87$ inferred in Section 3.4 using direct observations of the LyC emission.

To our knowledge, this is the first observational confirmation that large escape of ionizing photons strongly affects the strength of nebular lines and continuum emission in a star-forming galaxy, thereby its global SED, as predicted by Zackrisson et al. (2013). For the few LyC emitters known with $f_{\text{esc}}(\text{LyC}) \gtrsim 0.5$ (de Barros et al. 2016; Izotov et al. 2018b; Flury et al. 2022b), all of them show a combination of $EW_0(H\beta) (> 100 \text{ \AA})$ and β_{UV} that, according

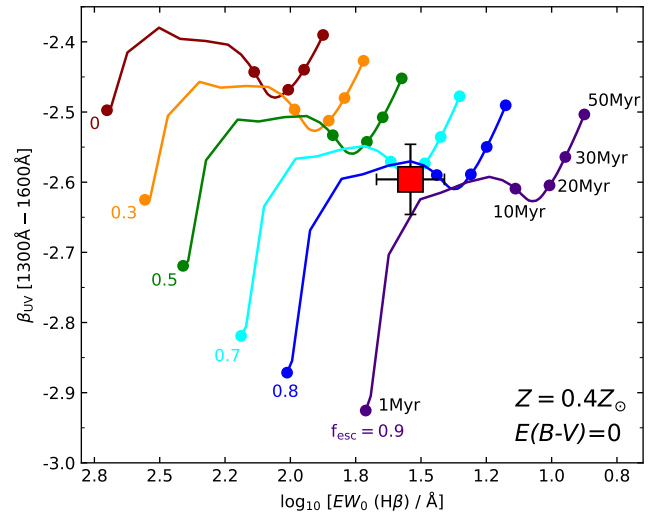


Figure 7. UV spectral slope (β_{UV}) and $H\beta$ equivalent width ($EW_0(H\beta)$) as a function of $f_{\text{esc}}(\text{LyC})$, predicted by S99 models with a continuous SFH with ages between 1 and 50 Myr and $Z = 0.4Z_{\odot}$. For the $H\beta$ emission we use the models of Schaerer & de Barros (2009) matched to the same stellar properties. The position of J1316+2614, marked with a red square, suggests large $f_{\text{esc}}(\text{LyC}) \simeq 0.8$ at the age of 9 Myr, and discards $f_{\text{esc}}(\text{LyC}) \leq 0.5$.

to the β_{UV} and $EW_0(H\beta)$ plane, are incompatible with the inferred $f_{\text{esc}}(\text{LyC})$ (e.g. see fig. 21 in Flury et al. 2022b). An exception could be Ion2 (Vanzella et al. 2016), which shows a very steep UV slope $\beta_{\text{UV}} = -2.7 \pm 0.6$ (de Barros et al. 2016) and $EW_0(H\beta) \simeq 100 \text{ \AA}$ (Vanzella et al. 2020), which according to Fig. 7 is compatible with very high $f_{\text{esc}}(\text{LyC})$, although with large uncertainties. It is known that the predicted tracks of $f_{\text{esc}}(\text{LyC})$ in the β_{UV} and $EW_0(H\beta)$ plane can be affected by different sources of uncertainty, such as the

effect of dust, stellar properties, star formation histories (Zackrisson et al. 2017), and ultimately by an inhomogeneous LyC leakage. For J1316+2614, these appear well constrained.

Finally, noting that J1316+2614 remains the only source known showing this behaviour (but see also J0121+0025 with $f_{\text{esc}}(\text{LyC}) \simeq 0.4$ and $EW_0(\text{Ly}\alpha) \simeq 14 \text{ \AA}$; Marques-Chaves et al. 2021, or Ion1 with no Ly α emission at all; Ji et al. 2020), our results highlight that at least some *weak* emission line galaxies with steep UV slopes could be potentially very strong LyC leakers. Our results do not contradict previous findings where $f_{\text{esc}}(\text{LyC})$ is found to correlate with the strength of nebular emission lines (e.g. $EW_0(\text{Ly}\alpha)$, $EW_0(\text{H}\beta + [\text{O III}])$, e.g. Izotov et al. 2016a; Flury et al. 2022b), at least up to moderately high $f_{\text{esc}}(\text{LyC})$. It rather indicates that the number of ionizing photons produced by the stellar population should be balanced with those contributing to the photoionization of H II regions and those escaping the galaxy, which can be critical at very high $f_{\text{esc}}(\text{LyC})$ (≥ 0.5).

4.2.2 H β luminosity

Another straightforward way to test $f_{\text{esc}}(\text{LyC})$ is to use the H β luminosity. Since H β is a recombination line and has little dependence on the metallicity and electron temperature (T_e) (e.g. Charlot & Longhetti 2001), it is basically a direct photons *counter*. Assuming $T_e = 10^4 \text{ K}$, the H β luminosity ($L(\text{H}\beta)$) can be expressed in terms of the production rate of ionizing photons, $Q_{\text{H}}^{\text{int}}$, and $f_{\text{esc}}(\text{LyC})$ by

$$\begin{aligned} L(\text{H}\beta) &= \frac{\gamma_{\text{H}\beta}}{\alpha_B} Q_{\text{H}}^{\text{int}} \times (1 - f_{\text{esc}}) \\ &= 2.1 \times 10^{12} Q_{\text{H}}^{\text{int}} \times (1 - f_{\text{esc}}), \end{aligned} \quad (3)$$

where $\gamma_{\text{H}\beta}$ is the nebular emission coefficient and α_B is the Case B recombination rate (Osterbrock & Ferland 2006). From the $Q_{\text{H}}^{\text{int}} = 8.5 \times 10^{55} \text{ s}^{-1}$ inferred in Section 3.4 and $L(\text{H}\beta) = (1.2 \pm 0.3) \times 10^{43} \text{ erg s}^{-1}$ derived from the observed H β flux (Table 2), we get $f_{\text{esc}}(\text{LyC}) = 0.82$, which matches almost perfectly with the direct measurement of $f_{\text{esc}}(\text{LyC})$.

4.2.3 Null covering fraction of neutral gas

Another piece of evidence for the high $f_{\text{esc}}(\text{LyC})$ is the absence of ISM low-ionization absorption lines in the spectrum of J1316+2614, which probe neutral gas in the line of sight (Gazagnes et al. 2018).

The spectra of typical LBGs or LAEs present typically relatively strong LIS lines, with $EW_0(\text{LIS}) \sim (1-4) \text{ \AA}$ (e.g. Shapley et al. 2003; Shibuya et al. 2014; Marques-Chaves et al. 2020a), but these are very weak or not detected in J1316+2614, as well as in other strong LyC leakers (Chisholm et al. 2017, 2018; Rivera-Thorsen et al. 2017; Izotov et al. 2018b; Marques-Chaves et al. 2021; Saldana-Lopez et al. 2022). The weakness of LIS lines in J1316+2614 could arise by a low geometric covering fraction of the gas, C_f , which would indicate a large $f_{\text{esc}}(\text{LyC})$, as $C_f = 1 - f_{\text{esc}}(\text{LyC})$ (e.g. Steidel et al. 2018). C_f can be inferred using the residual intensity of the absorption line, I , so that $C_f = 1 - I/I_0$, where I_0 is the continuum level.⁵ Assuming a line width of FWHM = 200 km s⁻¹, we infer $I/I_0 > 0.85$ and $EW_0(\text{LIS}) < 0.6 \text{ \AA}$ at 3σ confidence level for Si II 1260 \AA and C II 1334 \AA . A low geometric covering fraction of the gas is inferred for J1316+2614, $C_f < 0.15$ (3σ), which would be consistent

⁵This assumes the optically thick regime and an ionization-bounded ISM with a uniform dust-screen geometry.

with a high $f_{\text{esc}}(\text{LyC})$. Following the empirical correlation between the residual intensity of ISM LIS lines and $f_{\text{esc}}(\text{LyC})$ of Saldana-Lopez et al. (2022), we infer $f_{\text{esc}}(\text{LyC}) > 0.65$ (3σ). A low ion column density could also explain the weakness of LIS lines, but such scenario is unlikely, because these lines are almost always saturated in the spectra of star-forming galaxies, even in damped-Ly α systems with very low metallicities (e.g. Dessauges-Zavadsky et al. 2006).

4.2.4 Ly α spectral profile

Another common and well-studied tracer of $f_{\text{esc}}(\text{LyC})$ is the spectral shape and peak separation ($\Delta v(\text{Ly}\alpha)$) of the Ly α profile (e.g. Verhamme et al. 2015, 2017; Izotov et al. 2018b), which depends on the amount and geometry of the neutral gas and dust. Following Verhamme et al. (2015) and assuming a spherical homogeneous shell, the observed $\Delta v(\text{Ly}\alpha) = 680 \pm 70 \text{ km s}^{-1}$ in J1316+2614 suggests a large H I column density $N_{\text{HI}} \gtrsim 10^{20.5} \text{ cm}^{-2}$, implying $f_{\text{esc}}(\text{LyC}) \approx 0$ (Verhamme et al. 2017; Izotov et al. 2018b). A priori, this is incompatible with the $f_{\text{esc}}(\text{LyC}) \simeq 0.9$ directly measured from the LyC emission itself (Section 3.5). This suggests that J1316+2614 may have an inhomogeneous ISM geometry (e.g. clumpy) and/or complex gas dynamics.

With the available data it is not possible to draw any definitive conclusion on the connection between the Ly α profile and LyC leakage. The lack of LIS absorption lines in the spectrum of J1316+2614 (Section 4.2.3) indicates a low covering fraction of neutral gas in the line of sight. This is compatible with large $f_{\text{esc}}(\text{LyC}) \simeq 0.9$ observed in the spectrum of J1316+2614, and suggests a very low N_{HI} along the LyC source, $N_{\text{HI}} \lesssim 10^{16} \text{ cm}^{-2}$ (Verhamme et al. 2017). In such a case, Ly α would be preferentially seen at the systemic velocity (e.g. Naidu et al. 2022), but it should be highly suppressed too given the large escape of ionizing photons (similarly as H β , see Section 4.2.1). The Ly α profile seen in the $R \simeq 1800$ OSIRIS spectrum (Fig. 3) shows already $f_\lambda > 0$ at the systemic redshift, but the emission is faint and the limited resolution prevents us to properly resolve the line. It is thus possible that Ly α is being emitted from regions spatially offset from the LyC source, and if so, it could be offset and possibly more extended than the UV continuum.

The shape of the observed Ly α profile and the properties of the neutral gas inferred from it also depend on the intrinsic nebular profile, which is not well characterized with our data. The non-resonant lines H β and [O III] have relatively low SNR and are observed with low resolution (Fig. 5), not enough for a proper study of the intrinsic emission (e.g. to look for broad wings or complex structure of the line).

While higher spectral and spatial resolution observations of Ly α and non-resonant lines are required to investigate better the complex Ly α profile and its connection to the LyC in J1316+2614, our results already indicate that large $f_{\text{esc}}(\text{LyC})$ and large $\Delta v(\text{Ly}\alpha)$ can coexist. It is worth noting that similar large $\Delta v(\text{Ly}\alpha)$ have been observed in a few sources with evidence of LyC leakage. For example, the local infrared galaxy IRAS 01003–2238 studied in Martin et al. (2015) shows a remarkably similar Ly α profile as the one in J1316+2614, with a blue-to-red peak line ratio $I_{\text{blue}}/I_{\text{red}} > 1$ and similar peak separation. Complex kinematics with high-velocity wings are found both in Ly α and in non-resonant lines (e.g. H β), suggesting that scattering merely enhances the wings relative to the line core. Using radiative transfer modelling and assuming a clumpy geometry, Martin et al. (2015) found that the Ly α profile can be well explained by a low column density ($N_{\text{HI}} \simeq 10^{17} \text{ cm}^{-2}$), which is optically thin to

LyC. Another example is the LyC emitter Ion2 ($f_{\text{esc}}(\text{LyC}) \gtrsim 0.5$; de Barros et al. 2016; Vanzella et al. 2016), whose Ly α emission shows a peak separation of $\sim 550 \text{ km s}^{-1}$ when observed with relatively low resolution ($R \simeq 1200$, de Barros et al. 2016). Higher resolution observations ($R \simeq 5300$, Vanzella et al. 2020) reveal a much more complex Ly α profile, including a substantial emission at the systemic velocity.

Another important point worth mentioning is the difference between the Ly α and LyC escape fractions. While $f_{\text{esc}}(\text{Ly}\alpha) \geq f_{\text{esc}}(\text{LyC})$ is usually assumed and predicted (Kimm et al. 2019; Maji et al. 2022), J1316+2614 shows $f_{\text{esc}}(\text{Ly}\alpha) = 0.43 \pm 0.12$ (Section 3.4), which is $\sim 2\times$ lower than $f_{\text{esc}}(\text{LyC})$. However, we note that the Ly α emission represents only a small fraction (≈ 5 per cent) of the total LyC photons produced in J1316+2614, possibly indicating that the regions probed by Ly α could not be representative of those where LyC is escaping.

4.2.5 Other properties

Other observational signatures of J1316+2614 resemble those found in other LyC emitters. J1316+2614 shows a compact morphology, being not resolved in ground-based imaging. Assuming the $\simeq 1$ arcsec FWHM seeing conditions of optical images, we estimate an effective radius in the rest-frame UV $r_{\text{eff}} \leq 2 \text{ kpc}$. Considering the large SFR $\simeq 500 M_{\odot} \text{ yr}^{-1}$ inferred from the SED in Section 3.5, this implies a large SFR surface density $\Sigma\text{SFR} \geq 10 M_{\odot} \text{ yr}^{-1} \text{ kpc}^{-2}$, which is within the range of ΣSFR inferred in other strong LyC emitters (e.g. Vanzella et al. 2016; Izotov et al. 2018b; Marques-Chaves et al. 2021; Flury et al. 2022b). Such an intense, concentrated star formation and the expected feedback from stellar winds of massive stars and SN explosions could play a major role in shaping the ISM (e.g. Sharma et al. 2017), favouring the escape of ionizing photons. Although inflows appear to be the dominant kinematic pattern of the gas in J1316+2614, strong ionized outflows are also expected given the nature of J1316+2614 (e.g. Álvarez-Márquez et al. 2021). High SNR and high-resolution observations of the main rest-frame optical lines are required to investigate the presence of outflowing gas in J1316+2614.

On the other hand, J1316+2614 shows a relatively modest [O III]/[O II] line ratio, $O_{32} = 4.8 \pm 2.1$, at least compared to other strong leakers that show $O_{32} \gtrsim 10$ (e.g. de Barros et al. 2016; Izotov et al. 2018b). Using the empirical relation of Izotov et al. (2018a), the observed $O_{32} \simeq 5$ predicts $f_{\text{esc}}(\text{LyC}) \simeq 0.05$, which is inconsistent with our observations. However, this relation has been constrained using green pea LyC leakers with very low metallicities ($12 + \log(\text{O}/\text{H}) \leq 8.0$). As shown by Bassett et al. (2019), line ratios of $O_{32} \lesssim 5$ can still predict large $f_{\text{esc}}(\text{LyC}) \gtrsim 0.5$ if higher metallicities and/or lower ionization parameters are considered, which seems to be the case of J1316+2614 ($12 + \log(\text{O}/\text{H}) = 8.45 \pm 0.12$, see Section 3.3). This is also consistent with the recent results of Flury et al. (2022b), where a large scatter in O_{32} with $f_{\text{esc}}(\text{LyC})$ is found in low- z LyC emitters with a wide range of metallicities ($12 + \log(\text{O}/\text{H}) = 7.5\text{--}8.6$).

Finally, the spectrum of J1316+2614 shows strong P-Cygni profiles in wind lines (N V 1240 Å, C IV 1550 Å, and also O VI 1033 Å, see Figs 2 and 4) and these are ubiquitous in other strong LyC leakers (e.g. Borthakur et al. 2014; Izotov et al. 2016a, 2018a,b; Vanzella et al. 2018, 2020; Rivera-Thorsen et al. 2019; Marques-Chaves et al. 2021). While the presence of these spectral features does not necessarily imply LyC leakage, they indicate very young ages of the stellar population (e.g. Chisholm et al. 2019),

where the production of LyC photons from O-type stars and feedback from the strong winds and SN explosions are more efficient.

4.3 Favourable IGM transmission and/or high LyC production efficiency?

From the low-resolution OSIRIS spectrum we measure a ratio between the ionizing to non-ionizing flux density of $(f_{870}/f_{1500})_{\text{obs}} = 0.146 \pm 0.011$. This is a factor of $\simeq 2\text{--}3\times$ higher than those measured in other strong LyC emitters at $z \simeq 3$ (e.g. Fletcher et al. 2019; Pahl et al. 2021; Saxena et al. 2022), despite the fact that they are at lower redshifts and thereby, they might be less affected by IGM absorption than J1316+2614. Following equation (1) and the intrinsic ratio of the best-fitting S99 model, $(f_{870}/f_{1500})_{\text{int}} = 0.27$, we find that the IGM transmission in the spectral region probed by the LyC emission at $\lambda_0 = 830\text{--}910 \text{ \AA}$ should be $T(\text{IGM}) > 0.54$ to keep $f_{\text{esc}} \leq 1$. This is significantly larger than the mean $T(\text{IGM})$ expected at $z \simeq 3.5$ ($\langle T(\text{IGM}) \rangle \sim 0.2$, e.g. Inoue et al. 2014, Steidel et al. 2018, Bassett et al. 2021). Here, we investigate the probability to have such a favourable IGM transmission along the line of sight of J1316+2614.

We generate 10 000 model $z = 3.613$ sightlines simulating the distribution of H I absorbers using the TAOIST-MC code⁶ (Bassett et al. 2021). $T(\text{IGM})$ functions use the models of Inoue et al. (2014) and account for both intergalactic and circumgalactic medium (IGM+CGM) following the prescriptions of Steidel et al. (2018). For every model sightline, we derive the net transmission over the rest wavelength range $\lambda_0 = 830\text{--}910 \text{ \AA}$, the same interval used to measure the LyC flux of J1316+2614.

The left-hand panel of Fig. 8 shows the $T(\text{IGM})$ frequency distribution of these realizations. The bulk ($\simeq 80$ per cent) of the simulations have $T(\text{IGM}) < 0.4$. However, a small fraction of these models (148/10 000) shows a favourable IGM transmission (defined as $T(\text{IGM}) \geq 0.54$) which is compatible with $f_{\text{esc}} \leq 1$. The mean IGM transmission at $830\text{--}910 \text{ \AA}$ for the 10 000 models is found to be $T(\text{IGM})^{\text{mean}} \simeq 0.15$, while for the favourable sightlines is $T(\text{IGM})^{\text{fav}} \simeq 0.58$, which is similar to that measured between $\lambda_0 \simeq 950\text{--}1180 \text{ \AA}$ in Section 3.4 ($T(\text{IGM}) = 0.59 \pm 0.17$). Therefore, our results suggest that a favourable IGM transmission is still possible, although such occurrence has low probability ($P[T(\text{IGM}) \geq 0.54] \simeq 0.015$).

A relatively lower IGM transmission is still possible if the intrinsic ratio $(f_{870}/f_{1500})_{\text{int}}$ is higher than the one assumed from the best-fitting S99 model ($\simeq 0.27$), i.e. an SED with higher LyC production efficiency (ξ_{ion}). The right-hand panel of Fig. 8 shows the behaviour between $T(\text{IGM})$ and $(f_{870}/f_{1500})_{\text{int}}$ as a function of $f_{\text{esc}}(\text{LyC})$, following equation (1). Considering the mean IGM transmission at $z = 3.613$, $T(\text{IGM})^{\text{mean}} \simeq 0.15$, an intrinsic $(f_{870}/f_{1500})_{\text{int}} \geq 0.9$ is required to keep $f_{\text{esc}} \leq 1$, i.e. a source producing at least $\geq 3\times$ more ionizing photons than our best-fitting S99 model ($\xi_{\text{ion}} \gtrsim 25.9$).

Such high values of ξ_{ion} are disfavoured for J1316+2614 as the age and metallicity of the young stellar population are relatively well constrained ($9 \pm 5 \text{ Myr}$ and $Z/Z_{\odot} = 0.4$, Section 3.1). Considering a younger age (4 Myr) and lower metallicity ($Z/Z_{\odot} = 0.2$), $(f_{870}/f_{1500})_{\text{int}}$ would increase only a factor of $\simeq 20$ per cent than our fiducial S99 model. Also, the inclusion of binaries can increase $(f_{870}/f_{1500})_{\text{int}}$. Considering a BPASS models (v2.2, Stanway et al. 2016) with a continuous SFH with the same age (10 Myr), metallicity ($Z/Z_{\odot} = 0.4$), and IMF, the increase of $(f_{870}/f_{1500})_{\text{int}}$ is roughly around

⁶http://github.com/robbassett/TAOIST_MC/

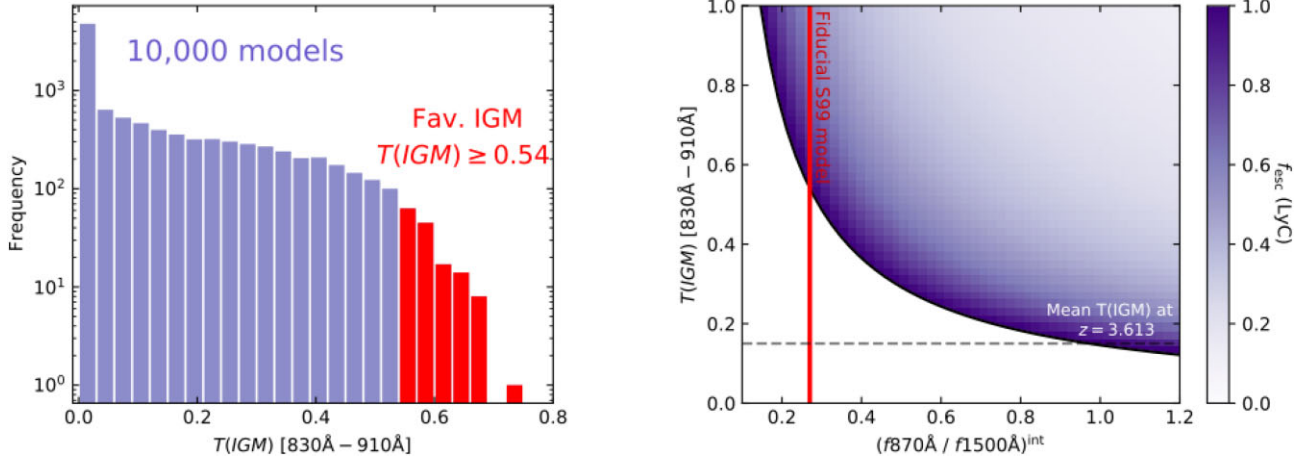


Figure 8. Left-hand panel: frequency distribution of the IGM transmission ($T(IGM)$) of 10 000 model sightlines simulating the distribution of H I absorbers at $z = 3.613$. These models were generated using TAOIST-MC code (Bassett et al. 2021) and $T(IGM)$ is computed between rest-frame wavelengths 830 and 910 Å. Only a small fraction of these models (148/10 000) predicts $T(IGM) \geq 0.54$, which is needed to keep $f_{esc} \leq 1$ in J1316+2614 (highlighted in red). Right-hand panel: relationship between $T(IGM)$ and $(f_{870}/f_{1500})^{int}$ as a function of f_{esc} (colour bar) following equation (1). The red vertical line is the $(f_{870}/f_{1500})^{int}$ inferred from the best-fitting S99 model (≈ 0.27). The horizontal dashed line is the mean $T(IGM)$ for the 10 000 models, $T(IGM) \approx 0.15$.

≈ 25 per cent when binaries are included. Finally, a different slope and a higher upper mass limit of the IMF can increase considerably $(f_{870}/f_{1500})^{int}$. Considering the most top-heavy IMF model available in the BPASS library, with an IMF slope of -2.0 and an upper mass limit of $300M_{\odot}$, and a continuous SFH with 10 Myr and $0.4Z_{\odot}$, we infer a $(f_{870}/f_{1500})^{int} \approx 0.46$ ($\xi_{ion} \approx 25.60$). In such a case, a $T(IGM) \geq 0.3$ is needed to keep $f_{esc} \leq 1$ (Fig. 8, right), i.e. still a factor of $\approx 2\times$ higher than the mean IGM transmission at $z = 3.613$.

In short, our results suggests that, even considering a stellar population with a higher $(f_{870}/f_{1500})^{int}$ and ξ_{ion} than that assumed for J1316+2614, a favourable IGM transmission and a large f_{esc} (LyC) are required to explain the LyC flux measured in this source.

Finally, the previous discussion on $(f_{870}/f_{1500})^{int}$, $T(IGM)$, and therefore f_{esc} (LyC) relies on the assumption that the observed LyC flux of J1316+2614 arises from the stellar emission itself, which might not be necessarily true. Models can predict the escape of free-bound emission of hydrogen in ionized nebulae from the radiation energy redistribution of stellar LyC (Inoue 2010). Under certain conditions [e.g. high electron temperature and f_{esc} (LyC), hard stellar SED, see details in Inoue 2010], this emission can be strong, producing a ‘Lyman bump’ seen just below of the Lyman edge ($\lesssim 912$ Å). If present in J1316+2614, the f_{esc} (LyC) inferred in Section 3.1 could be overestimated, although it should be high. The limited SNR and spectral coverage of our OSIRIS spectrum in the LyC region, along with the inherent uncertainties due to IGM, prevent us to further investigate the presence of this ‘Lyman bump’ emission in J1316+2614. Nevertheless, its presence could explain the absence of the Lyman break around ≈ 912 Å in the spectrum of J1316+2614 (see Fig. 4), which is expected if only pure stellar models are assumed.

4.4 The most powerful ionizing source known among star-forming galaxies

We now proceed to compare the f_{esc} (LyC) and the UV absolute magnitude of J1316+2614 with other LyC emitters. Fig. 9 shows the f_{esc} (LyC) and M_{UV} of J1316+2614 (magenta) and other ~ 40 individual LyC emitters with direct detection of LyC radiation. The comparison sample consists of both low redshift ($z \sim 0.3$, Izotov

et al. 2016a,b, 2018a,b; Flury et al. 2022b, open circles) and $z > 2$ star-forming galaxies (Shapley et al. 2016; Vanzella et al. 2016, 2018, 2020; Fletcher et al. 2019; Marques-Chaves et al. 2021; Saxena et al. 2022, filled circles). The figure also includes several statistical results of f_{esc} (LyC) from deep imaging and spectral stacks of LBGs and LAEs (Grazian et al. 2017; Marchi et al. 2017; Rutkowski et al. 2017; Fletcher et al. 2019; Bian & Fan 2020; Pahl et al. 2021; Begley et al. 2022, green diamonds). Most of these stacks show upper limits on f_{esc} (LyC) from ~ 0.2 to a few per cent.

As seen in this figure, the inferred f_{esc} (LyC) ≈ 0.87 of J1316+2614 places it among the most powerful LyC emitter known. This result is robust and should not depend significantly with the assumptions on the IGM attenuation. Even assuming a completely transparent (and unrealistic) IGM for J1316+2614, $T(IGM) = 1$, we would still infer f_{esc} (LyC) ≈ 0.54 (Section 3.4), which is larger than in many other LyC emitters. Therefore, our results indicate that large f_{esc} (LyC) can be found in UV-bright star-forming galaxies, and are not restricted to the faintest ones as previously thought, as already discussed in Marques-Chaves et al. (2021). Previous studies have found a possible anticorrelation between f_{esc} (LyC) and M_{UV} (Steidel et al. 2018; Pahl et al. 2021; Saldana-Lopez et al. 2022), i.e. f_{esc} (LyC) decreases towards UV-brighter sources, but these works probe relatively faint galaxies with a narrow range of UV absolute magnitudes ($M_{UV} \sim -20 \pm 1$). To our knowledge there are no statistical studies probing f_{esc} (LyC) of star-forming galaxies brighter than $M_{UV} < -22$. The few exceptions are the ones presented in Grazian et al. (2017) where f_{esc} (LyC) < 0.08 (3σ) is found for $M_{UV} \sim -23$, but their sample consists of two sources only. Fig. 9 clearly shows that several UV-bright sources ($M_{UV} < -22$, Vanzella et al. 2018; Marques-Chaves et al. 2021; Saxena et al. 2022), including J1316+2614, are very strong LyC emitters.

It is worth discussing that many properties inferred for J1316+2614 and in other UV-bright LyC emitters (Vanzella et al. 2018; Marques-Chaves et al. 2021) are remarkably similar as those found in UV-faint leakers (e.g. Izotov et al. 2018b). These include very young ages ($\lesssim 10$ Myr), high $sSFR$ (~ 100 Gyr $^{-1}$), compact morphologies, and low dust attenuation, among others (e.g. weak UV absorption lines, strong wind lines, etc.). The remarkable difference between them is the ≈ 4 – 5 mag in the UV, which is related to the

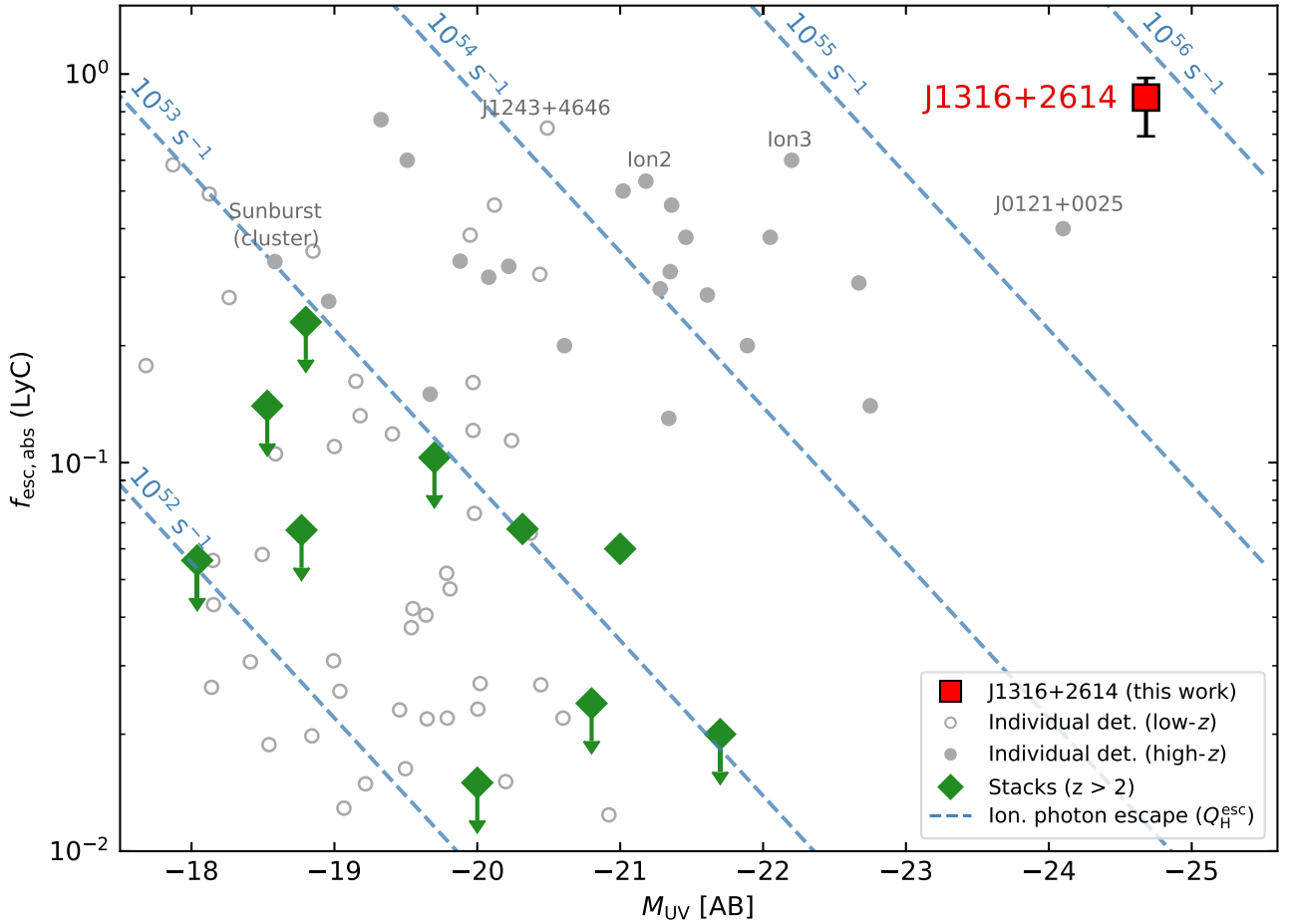


Figure 9. Relation between the absolute LyC escape fraction, f_{esc} (LyC), and UV absolute magnitude, M_{UV} (AB). J1316+2614 is represented with a red square. Other ~ 40 individual star-forming galaxies with direct detection of LyC are also shown. These include $z \sim 0.3$ sources (Izotov et al. 2016a,b, 2018a,b; Flury et al. 2022a, open circles) and other star-forming galaxies at $z > 2$ (Shapley et al. 2016; Vanzella et al. 2016, 2018, 2020; Fletcher et al. 2019; Rivera-Thorsen et al. 2019; Marques-Chaves et al. 2021; Saxena et al. 2022, filled circles). Results from deep stacks are marked with green diamonds (Grazian et al. 2017; Marchi et al. 2017; Rutkowski et al. 2017; Fletcher et al. 2019; Bian & Fan 2020; Pahl et al. 2021; Begley et al. 2022). The blue dashed lines show the ionizing photon escape, Q_H^{esc} , predicted for a given M_{UV} and f_{esc} (LyC) assuming the ionizing photon production efficiency derived for J1316+2614 ($\log(\xi_{\text{ion}}/\text{erg}^{-1}\text{Hz}) = 25.40$). J1316+2614 is by far the most powerful ionizing source known among the star-forming galaxies, both in terms of f_{esc} (LyC) and Q_H^{esc} .

strength or amplitude of the burst. The Ly α profile of J1316+2614 also differs from those observed in other LyC leakers, showing typically a red-dominated peak and $\Delta v(\text{Ly}\alpha) \lesssim 250 \text{ km s}^{-1}$ (e.g. Izotov et al. 2018b). It is still unclear if the properties governing the escape of ionizing photons of these UV-bright galaxies are similar to those of UV-faint sources, but should be further explored with larger samples of UV-bright sources.

Another important output from Fig. 9 is the ionizing photon escape (Q_H^{esc}) predicted for a given M_{UV} and f_{esc} (LyC). This is highlighted by the dashed lines in Fig. 9. For simplicity, these lines assume the ionizing photon production efficiency derived for J1316+2614, $\log(\xi_{\text{ion}}/\text{erg}^{-1}\text{Hz}) = 25.40$. We caution that the assumed ξ_{ion} may differ from source to source depending on galaxy properties (e.g. metallicity, age, SFH). For example, some UV-faint, low-metallicity starbursts at low z , including LyC emitters, present higher ξ_{ion} (e.g. $\log(\xi_{\text{ion}}/\text{erg}^{-1}\text{Hz}) \simeq 25.8$, Schaerer et al. 2016), while more typical $z \sim 2-5$ LBGs and LAEs show $\log(\xi_{\text{ion}}/\text{erg}^{-1}\text{Hz}) \simeq 24.8 - 25.4$ (e.g. Bouwens et al. 2016; Matthee et al. 2017). Despite the differences in the assumed ξ_{ion} , Fig. 9 shows that the ionizing photon escape of J1316+2614 ($Q_H^{\text{esc}} \approx (7-8) \times 10^{55} \text{ s}^{-1}$, Section 3.5) is orders of magnitude higher than those predicted in UV-faint sources, even those showing large f_{esc} (LyC). The differences are even more extreme

if the results from deep stacks of typical LBGs and LAEs are considered, where LyC emission is usually not detected down to f_{esc} (LyC) of a few per cent (Rutkowski et al. 2017; Fletcher et al. 2019). The Q_H^{esc} inferred for J1316+2614 is $\geq 10^3-10^4$ higher than that inferred for stacks of LAE/LBG population.

The combination of large production and escape of LyC photons makes J1316+2614 the most powerful ionizing source known among star-forming galaxies, only comparable to J0121+0025 at $z = 3.24$ ($M_{\text{UV}} = -24.2$ and $f_{\text{esc}}(\text{LyC}) \approx 0.4$; Marques-Chaves et al. 2021). Whether or not these UV-luminous star-forming galaxies can contribute to the cosmic reionization at higher redshifts ($z \gtrsim 6$), locally or globally, is still unclear and depends fundamentally if such sources are present in the early Universe and on their number density. Recent works have found exceptionally luminous ($M_{\text{UV}} \lesssim -23$) sources at $z \geq 6$ with properties resembling those seen in strong LyC leakers, such as compact morphologies, steep UV slopes, or high sSFRs (e.g. Morishita et al. 2020; Bouwens et al. 2022b; Harikane et al. 2022b). However, the inferred number density of these sources is still largely uncertain, ranging from $\lesssim 10^{-7}$ to some 10^{-6} Mpc^{-3} for $M_{\text{UV}} \simeq -23$ at $z \simeq 7-8$ (e.g. Calvi et al. 2016; Bowler et al. 2020; Rojas-Ruiz et al. 2020; Finkelstein & Bagley 2022; Leethochawalit et al. 2022).

4.5 Massive inflows feeding a UV-luminous starburst

J1316+2614 is the most luminous star-forming galaxy known in the UV ($M_{\text{UV}} = -24.68 \pm 0.08$) and Ly α ($\log(L[\text{Ly}\alpha/\text{erg s}^{-1}]) = 44.09 \pm 0.10$). We have shown that the large luminosity is powered by a young ($\simeq 10$ Myr) stellar population with $M_*/M_{\odot} \simeq 10^{9.7}$ and $\text{SFR} \simeq 500 M_{\odot} \text{ yr}^{-1}$ (Table 4), without any evidence of AGN activity. This yields a very high $s\text{SFR} \simeq 105 \text{ Gyr}^{-1}$ if only the mass of the young stellar population is assumed. Here, we discuss possible mechanisms that could explain the intense starburst nature of J1316+2614.

With the available data we do not find any hint of a major merger that could enhance the SFR observed in J1316+2614. The morphology of J1316+2614 appears compact ($r_{\text{eff}} \leq 2 \text{ kpc}$), and in addition, merger-induced SFRs are usually low, a factor of 2 at most (e.g. Pearson et al. 2019). Rather than that, the rest-frame UV spectrum of J1316+2614 shows signs of inflowing gas and these are likely related to its recent SFH. The spectral shape of the Ly α emission in J1316+2614, with a blue peak more intense than the red one (Fig. 3), and the redshifted ISM absorption of C IV (Fig. 2) suggest gas inflows. Only a few star-forming galaxies are known to show similar Ly α profiles (e.g. Trainor et al. 2015, Izotov et al. 2020), but with much lower SNR. The redshifted ISM absorption lines have been also found in the spectra of star-forming galaxies at moderately low z (with a ~ 5 per cent–6 per cent detection rates, e.g. Martin et al. 2012, Rubin et al. 2012), but are more elusive at high z (e.g. Falgarone et al. 2017, Marques-Chaves et al. 2018, Herrera-Camus et al. 2020), possibly due to cosmological dimming and low-SNR continuum spectra.

Cosmological simulations predict that massive inflows towards a central star-forming region from wet disc compaction may be frequent in high-redshift galaxies (Dekel & Burkert 2014; Zolotov et al. 2015; Dekel et al. 2020). Violent disc instabilities, counter-rotating gas, gas-rich (minor) mergers, recycled gas inflows from galactic fountains may provoke a dissipative shrinkage of gaseous discs, triggering the star formation in the central part of the galaxy, increasing the $s\text{SFR}$ and gas density. This event is usually referred to the ‘blue nugget’ phase. At later times, this can eventually lead to central depletion and quenching of the star formation (e.g. Tacchella et al. 2016b), resulting in a compact quiescent galaxy (red nugget).

We speculate that a similar mechanism could be responsible for the massive starburst observed in J1316+2614. Fig. 10 shows a schematic illustration of this mechanism that helps to explain and visualize several properties observed in J1316+2614. Gas contraction or neutral gas inflows in J1316+2614 (left) would lead to an intense and concentrated star formation episode, increasing the $s\text{SFR}$ and ΣSFR in a short period of time of a few Myr (right). This could explain the recent and bursty SFH, large luminosity, SFR, and the overall SED of J1316+2614 (right). The inflowing gas that we observed in J1316+2614 could correspond to gas left that has not been converted into stars. Gas in the remaining regions could have been consumed already in the starburst or removed by stellar winds and supernovae feedback. These regions would present low column density of neutral gas, $N_{\text{HI}} \lesssim 10^{16} \text{ cm}^{-2}$, where LyC photons are escaping.

Simulations predict that the maximum compaction of the gaseous disc occurs at stellar masses $\sim 10^{9.5} M_{\odot}$ at $z \sim 2\text{--}4$ (Tacchella et al. 2016b), which is broadly consistent with that inferred for J1316+2614 ($M_*/M_{\odot} \simeq 10^{9.67}$). Simulations also predict that the maximum increase of the $s\text{SFR}$ with respect to the MS is $\Delta\log(s\text{SFR}) \simeq 0.3\text{--}0.7$ in the compaction phase (Zolotov et al.

2015; Tacchella et al. 2016a), while for J1316+2614 we infer $\Delta\log(s\text{SFR}) \simeq 1.5$ if only the mass formed in the most recent SFH is considered. This suggests the presence of an old stellar population, which according to our results inferred in Section 3.5 should be less massive than $M_*^{\text{old}}/M_{\odot} \leq 10^{10.3}$ (5σ). If both young and old stellar components are considered, the specific SFR can decrease considerably, down to $s\text{SFR} \geq 20 \text{ Gyr}^{-1}$ or ≥ 0.6 dex above the MS (Fig. 5), but still consistent with simulations (Zolotov et al. 2015; Tacchella et al. 2016a).

The violent star formation episode observed in J1316+2614 resemble those of some massive and quiescent galaxies found at $z \gtrsim 3$, where strong ($\text{SFR} \gtrsim 1000 M_{\odot} \text{ yr}^{-1}$) and short (~ 50 Myr) events of star formation are invoked (e.g. Glazebrook et al. 2017; Forrest et al. 2020; Valentino et al. 2020). Other works have identified compact star-forming galaxies with morphological properties and colours that are expected in the progenitors of quiescent and massive galaxies (e.g. Barro et al. 2013, 2017; Huertas-Company et al. 2018), but without the information on the gas kinematics. At some extent, similar mechanisms are required to explain the properties of the two star-forming galaxies known brighter than $M_{\text{UV}} < -24.0$, BOSS-EUVLG1 at $z = 2.47$ ($M_{\text{UV}} = -24.4$; Marques-Chaves et al. 2020b) and J0121+0025 at $z = 3.24$ ($M_{\text{UV}} = -24.2$, also a LyC leaker; Marques-Chaves et al. 2021), both selected in the same way as J1316+2614 using the public BOSS/SDSS survey. These sources share similar properties as J1316+2614, characterized by young ($\lesssim 10$ Myr) starbursts with $\text{SFR} \simeq 1000 M_{\odot} \text{ yr}^{-1}$, $s\text{SFR} \simeq 100 \text{ Gyr}^{-1}$, and compact morphologies ($r_{\text{eff}} \simeq 1 \text{ kpc}$). Nevertheless, neutral and ionized outflows are detected in BOSS-EUVLG1 and J0121+0025 (Marques-Chaves et al. 2020b, 2021; Álvarez-Márquez et al. 2021), without any evidence for the inflowing signatures that we observe in J1316+2614, but are also expected due to the increase of $s\text{SFR}$ and ΣSFR in these sources (e.g. Williams et al. 2015).

In short, J1316+2614 and the other UV-bright star-forming galaxies discovered recently (Marques-Chaves et al. 2020b, 2021) could represent the initial phases (~ 10 Myr) in the evolution of massive galaxies. Their fate will depend on the amount of gas available and the efficiency to form new stars, which are still unknown. Star formation can be quenched by starvation or they can continue to form new stars and dust, possibly reaching the far-IR bright phase. Other physical processes, e.g. major merger, formation of a super massive black hole, or its ignition and feedback, could alter their fate as well. In any case, these UV-luminous phases must be short lived, lasting some tens to a few hundreds Myr, as already discussed in Marques-Chaves et al. (2020b), but should mark drastic transitions on the properties of these galaxies, on the stellar mass build-up, chemical an dust enrichment, quenching mechanisms, and possibly on LyC leakage.

5 CONCLUSION

In this work, we have presented the discovery and analysis of J1316+2614 at $z = 3.613$, a luminous star-forming galaxy with high escape fraction of LyC radiation. While selected first as a bright QSO within BOSS/SDSS, follow-up observations with the GTC have revealed its true, starburst nature without any signs of AGN activity. From the analysis of these data we arrive at the following main results:

(i) J1316+2614 is the most luminous star-forming galaxy known so far in the UV and Ly α , with $M_{\text{UV}} = -24.68 \pm 0.08$ and $\log(L[\text{Ly}\alpha/\text{erg s}^{-1}]) = 44.09 \pm 0.10$. The detection of stellar features in the rest-frame UV spectrum, such as photospheric absorption lines

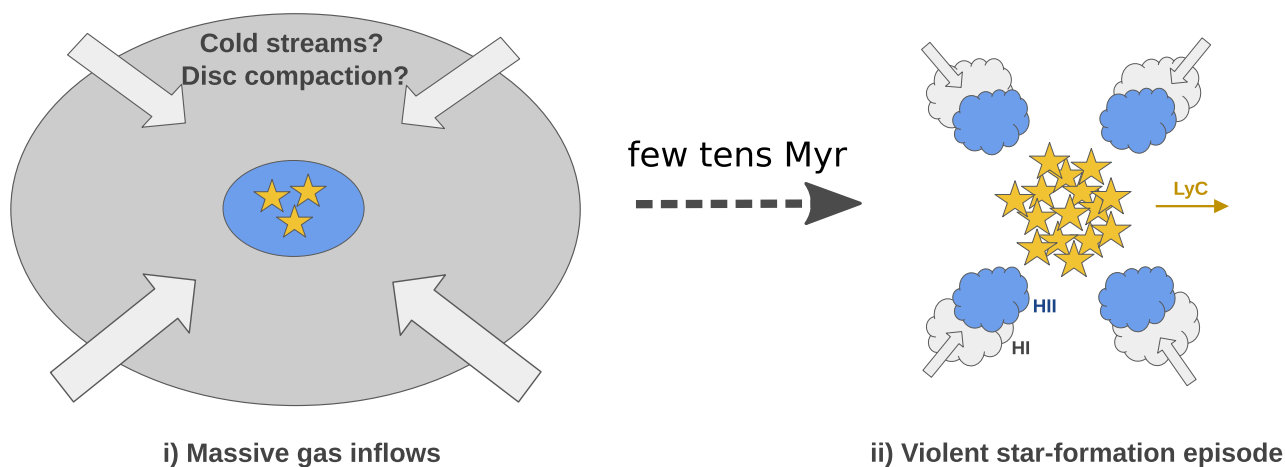


Figure 10. Schematic temporal evolution of the proposed mechanism responsible for the massive starburst observed in J1316+2614. (i) Disc contraction or bulk neutral gas inflows in J1316+2614 (left) would lead to (ii) an intense and concentrated star formation in a short period of time of a few Myr (right), increasing the $sSFR$ and ΣSFR . The right-hand panel also shows a schematic distribution and kinematics of the gas. LyC photons (yellow arrow) would escape from regions with low column density of neutral gas, $N_{\text{HI}} \lesssim 10^{16} \text{ cm}^{-2}$.

and wind lines, narrow nebular emission ($< 500 \text{ km s}^{-1}$), and blue SED ($\beta_{\text{UV}} = -2.59 \pm 0.05$, $r - W1 < -0.3$), discards a dominant AGN contribution to the luminosity of J1316+2614. We do not find any evidence of J1316+2614 being magnified by gravitational lensing.

(ii) The rest-frame UV spectrum is well reproduced by an S99 model with a continuous SFH with an age of 9 Myr, $Z_*/Z_{\odot} \simeq 0.4$ and little dust obscuration ($E(B - V) = 0.006^{+0.018}_{-0.006}$). The corresponding ionizing photon production efficiency is $\log(\xi_{\text{ion}}[\text{Hz erg}^{-1}]) \approx 25.40$. The optical to mid-IR photometry (0.1–1.0 μm , rest) is dominated by the emission of this young stellar population. Our multiwavelength best-fitting SED model predicts an $SFR = 497 \pm 92 M_{\odot} \text{ yr}^{-1}$ and $\log(M_*/M_{\odot}) = 9.67 \pm 0.07$ for the young stellar population. The presence of an old stellar population ($\geq 200 \text{ Myr}$) is not well constrained, but should be less massive than $\log(M_*/M_{\odot}) \leq 10.3$ (5σ).

(iii) LyC emission ($\lambda_0 < 912 \text{ \AA}$) is significantly detected down to 830 \AA and with a mean flux density $f_{\text{LyC}} = 1.69 \pm 0.10 \mu\text{Jy}$. We infer a relative (absolute) LyC escape fraction $f_{\text{esc}}(\text{LyC}) \simeq 0.92$ ($\simeq 0.87$) assuming a relatively high IGM transmission ($\simeq 0.59$). The contribution of a foreground or AGN contamination to the LyC signal is unlikely. Other indirect tracers also suggest high escape fraction, including high specific SFR ($sSFR = 105 \pm 49 \text{ Gyr}^{-1}$) and SFR surface density ($\Sigma SFR \geq 10 M_{\odot} \text{ yr}^{-1} \text{ kpc}^{-2}$), and weak/non-detected LIS lines. J1316+2614 is the most powerful ionizing source known among the star-forming galaxy population, both in terms of production ($Q_{\text{H}} \approx 10^{56} \text{ s}^{-1}$) and escape ($f_{\text{esc}}(\text{LyC}) \approx 0.9$) of ionizing photons.

(iv) Nebular emission is detected in Ly α and in rest-frame optical lines H β , [OII], and [OIII], but these are much weaker (EW_0 's of Ly α and H β of $\simeq 20$ – 30 \AA) than that expected for the derived SFH of J1316+2614 ($EW \geq 120 \text{ \AA}$ for $\simeq 10 \text{ Myr}$ age). Our results demonstrate, for the first time, that large escape of ionizing photons affects strongly the strength of nebular lines and continuum emission, roughly by a factor of $(1 - f_{\text{esc}}(\text{LyC}))$, and that only a fraction of ionizing photons will contribute to the photoionization of HII regions. This suggests that at least some weak emission line galaxies could be potentially very strong LyC leakers. This may help in designing future surveys to detect very strong LyC emitters, which are for now restricted mostly in targeting extreme emission line star-forming galaxies, like green pea-like galaxies.

(v) The Ly α emission in J1316+2614 shows a double-peaked profile, with a blue peak more intense than the red one ($I_{\text{blue}}/I_{\text{red}} = 3.7 \pm 0.1$) indicating neutral gas inflows. This is supported by the detection of redshifted ISM components of CIV. We speculate that massive inflows or dissipative compaction of the gas disc have triggered an intense and concentrated star formation in the central part of the J1316+2614 and in a short period of time. This would explain its recent SFH, as well as many other properties observed in J1316+2614, such as its large luminosity, SFR, $sSFR$, ΣSFR , SED, and gas kinematics. J1316+2614 may represent the first case known of a star-forming galaxy undergoing a ‘blue nugget’ phase, where gas inflows and a massive, compact, and young starburst are observed simultaneously.

ACKNOWLEDGEMENTS

The authors thank the anonymous referee for useful comments that greatly improved the clarity of this work. RMC thanks Fabrice Martins, Benjamin Magnelli, and Jorge Sanchez-Almeida for useful discussions. Based on observations made with the Gran Telescopio Canarias (GTC) installed in the Spanish Observatorio del Roque de los Muchachos of the Instituto de Astrofísica de Canarias, in the island of La Palma. JAM, LC, and IPF acknowledge support from the Spanish State Research Agency (AEI) under grant numbers ESP2015-65597-C4-4-R, ESP2017-86852-C4-2-R, PID2021-127718NB-I00, PGC2018-094975-B-C22, and MDM-2017-0737 Unidad de Excelencia ‘María de Maeztu’- Centro de Astrobiología (CSIC-INTA). DC is a Ramon-Cajal Researcher and is supported by the Ministerio de Ciencia, Innovación y Universidades (MICIU/FEDER) under research grant PID2021-122603NB-C21. ASL acknowledges support from Swiss National Science Foundation. ASL acknowledges support from Swiss National Science Foundation.

DATA AVAILABILITY

The data underlying this article will be shared on reasonable request to the corresponding author.

REFERENCES

- Abolfathi B. et al., 2018, *ApJS*, 235, 42
- Alexandroff R. M., Heckman T. M., Borthakur S., Overzier R., Leitherer C., 2015, *ApJ*, 810, 104
- Álvarez-Márquez J., Marques-Chaves R., Colina L., Pérez-Fournon I., 2021, *A&A*, 647, A133
- Ao Y. et al., 2020, *Nat. Astron.*, 4, 670
- Bañados E. et al., 2018, *Nature*, 553, 473
- Barro G. et al., 2013, *ApJ*, 765, 104
- Barro G. et al., 2017, *ApJ*, 840, 47
- Bassett R. et al., 2019, *MNRAS*, 483, 5223
- Bassett R., Ryan-Weber E. V., Cooke J., Meštrić U., Kakiichi K., Prichard L., Rafelski M., 2021, *MNRAS*, 502, 108
- Begley R. et al., 2022, *MNRAS*, 513, 3510
- Bian F., Fan X., 2020, *MNRAS*, 493, L65
- Boquien M., Burgarella D., Roehly Y., Buat V., Ciesla L., Corre D., Inoue A. K., Salas H., 2019, *A&A*, 622, A103
- Borthakur S., Heckman T. M., Leitherer C., Overzier R. A., 2014, *Science*, 346, 216
- Bouwens R. J., Smit R., Labbé I., Franx M., Caruana J., Oesch P., Stefanon M., Rasappu N., 2016, *ApJ*, 831, 176
- Bouwens R. J., Illingworth G. D., van Dokkum P. G., Oesch P. A., Stefanon M., Ribeiro B., 2022a, *ApJ*, 927, 81
- Bouwens R. J. et al., 2022b, *ApJ*, 931, 160
- Bowler R. A. A., Jarvis M. J., Dunlop J. S., McLure R. J., McLeod D. J., Adams N. J., Milvang-Jensen B., McCracken H. J., 2020, *MNRAS*, 493, 2059
- Bruzual G., Charlot S., 2003, *MNRAS*, 344, 1000
- Burgarella D., Buat V., Iglesias-Páramo J., 2005, *MNRAS*, 360, 1413
- Calvi V. et al., 2016, *ApJ*, 817, 120
- Calzetti D., Armus L., Bohlin R. C., Kinney A. L., Koornneef J., Storchi-Bergmann T., 2000, *ApJ*, 533, 682
- Cardelli J. A., Clayton G. C., Mathis J. S., 1989, *ApJ*, 345, 245
- Chabrier G., 2003, *ApJ*, 586, L133
- Charlot S., Longhetti M., 2001, *MNRAS*, 323, 887
- Chisholm J., Orlitová I., Schaerer D., Verhamme A., Worseck G., Izotov Y. I., Thuan T. X., Guseva N. G., 2017, *A&A*, 605, A67
- Chisholm J. et al., 2018, *A&A*, 616, A30
- Chisholm J., Rigby J. R., Bayliss M., Berg D. A., Dahle H., Gladders M., Sharon K., 2019, *ApJ*, 882, 182
- Chisholm J. et al., 2022, preprint ([arXiv:2207.05771](https://arxiv.org/abs/2207.05771))
- Cristiani S., Serrano L. M., Fontanot F., Vanzella E., Monaco P., 2016, *MNRAS*, 462, 2478
- Crowther P. A. et al., 2016, *MNRAS*, 458, 624
- Daddi E. et al., 2021, *A&A*, 649, A78
- de Barros S. et al., 2016, *A&A*, 585, A51
- Dekel A., Burkert A., 2014, *MNRAS*, 438, 1870
- Dekel A. et al., 2020, *MNRAS*, 496, 5372
- Dessauges-Zavadsky M., Prochaska J. X., D'Odorico S., Calura F., Matteucci F., 2006, *A&A*, 445, 93
- Dijkstra M., Haiman Z., Spaans M., 2006, *ApJ*, 649, 14
- Eisenstein D. J. et al., 2011, *AJ*, 142, 72
- Endsley R., Stark D. P., Chevillard J., Charlot S., 2021, *MNRAS*, 500, 5229
- Erb D. K. et al., 2014, *ApJ*, 795, 33
- Falgarone E. et al., 2017, *Nature*, 548, 430
- Finkelstein S. L., Bagley M. B., 2022, preprint ([arXiv:2207.02233](https://arxiv.org/abs/2207.02233))
- Finkelstein S. L. et al., 2019, *ApJ*, 879, 36
- Fletcher T. J., Tang M., Robertson B. E., Nakajima K., Ellis R. S., Stark D. P., Inoue A., 2019, *ApJ*, 878, 87
- Flury S. R. et al., 2022a, *ApJS*, 260, 1
- Flury S. R. et al., 2022b, *ApJ*, 930, 126
- Forrest B. et al., 2020, *ApJ*, 890, L1
- Furtak L. J. et al., 2022, *MNRAS*, 516, 1373
- Garcia M., Bianchi L., 2004, *ApJ*, 606, 497
- Gazagnes S., Chisholm J., Schaerer D., Verhamme A., Rigby J. R., Bayliss M., 2018, *A&A*, 616, A29
- Glazebrook K. et al., 2017, *Nature*, 544, 71
- Grazian A. et al., 2017, *A&A*, 602, A18
- Harikane Y. et al., 2022a, *ApJS*, 259, 20
- Harikane Y. et al., 2022b, *ApJ*, 929, 1
- Hashimoto T. et al., 2019, *PASJ*, 71, 71
- Herrera-Camus R. et al., 2020, *A&A*, 633, L4
- Huertas-Company M. et al., 2018, *ApJ*, 858, 114
- Inoue A. K., 2010, *MNRAS*, 401, 1325
- Inoue A. K., Iwata I., 2008, *MNRAS*, 387, 1681
- Inoue A. K., Shimizu I., Iwata I., Tanaka M., 2014, *MNRAS*, 442, 1805
- Izotov Y. I., Schaerer D., Thuan T. X., Worseck G., Guseva N. G., Orlitová I., Verhamme A., 2016a, *MNRAS*, 461, 3683
- Izotov Y. I., Orlitová I., Schaerer D., Thuan T. X., Verhamme A., Guseva N. G., Worseck G., 2016b, *Nature*, 529, 178
- Izotov Y. I., Schaerer D., Worseck G., Guseva N. G., Thuan T. X., Verhamme A., Orlitová I., Fricke K. J., 2018a, *MNRAS*, 474, 4514
- Izotov Y. I., Worseck G., Schaerer D., Guseva N. G., Thuan T. X., Fricke Verhamme A., Orlitová I., 2018b, *MNRAS*, 478, 4851
- Izotov Y. I., Schaerer D., Worseck G., Verhamme A., Guseva N. G., Thuan T. X., Orlitová I., Fricke K. J., 2020, *MNRAS*, 491, 468
- Jaskot A. E., Oey M. S., 2013, *ApJ*, 766, 91
- Ji Z. et al., 2020, *ApJ*, 888, 109
- Kimm T., Blaizot J., Garel T., Michel-Dansac L., Katz H., Rosdahl J., Verhamme A., Haehnelt M., 2019, *MNRAS*, 486, 2215
- Leethochawalit N., Roberts-Borsani G., Morishita T., Trenti M., Treu T., 2022, preprint ([arXiv:2205.15388](https://arxiv.org/abs/2205.15388))
- Leitherer C. et al., 1999, *ApJS*, 123, 3
- Li Z., Steidel C. C., Gronke M., Chen Y., Matsuda Y., 2022, *MNRAS*, 513, 3414
- Lin Y.-H., Scarlata C., Hayes M., Feltre A., Charlot S., Bongiorno A., Väisänen P., Mogotsi M., 2022, *MNRAS*, 509, 489
- Liu C. et al., 2022, *ApJS*, 261, 24
- Lusso E., Worseck G., Hennawi J. F., Prochaska J. X., Vignali C., Stern J., O'Meara J. M., 2015, *MNRAS*, 449, 4204
- Maji M. et al., 2022, *A&A*, 663, A66
- Marchi F. et al., 2017, *A&A*, 601, A73
- Marocco F. et al., 2021, *ApJS*, 253, 8
- Marques-Chaves R. et al., 2018, *ApJ*, 854, 151
- Marques-Chaves R. et al., 2020a, *MNRAS*, 492, 1257
- Marques-Chaves R. et al., 2020b, *MNRAS*, 499, L105
- Marques-Chaves R., Schaerer D., Álvarez-Márquez J., Colina L., Dessauges-Zavadsky M., Pérez-Fournon I., Saldana-Lopez A., Verhamme A., 2021, *MNRAS*, 507, 524
- Marques-Chaves R. et al., 2022, *A&A*, 663, L1
- Martin C. L., Shapley A. E., Coil A. L., Kornei K. A., Bundy K., Weiner B. J., Noeske K. G., Schiminovich D., 2012, *ApJ*, 760, 127
- Martin C. L., Dijkstra M., Henry A., Soto K. T., Danforth C. W., Wong J., 2015, *ApJ*, 803, 6
- Martins F., Palacios A., 2022, *A&A*, 659, A163
- Maseda M. V. et al., 2020, *MNRAS*, 493, 5120
- Mason C. A., Treu T., Dijkstra M., Mesinger A., Trenti M., Pentericci L., de Barros S., Vanzella E., 2018, *ApJ*, 856, 2
- Matthee J., Sobral D., Best P., Khostovan A. A., Oteo I., Bouwens R., Röttgering H., 2017, *MNRAS*, 465, 3637
- Micheva G., Iwata I., Inoue A. K., 2017, *MNRAS*, 465, 302
- Morishita T. et al., 2020, *ApJ*, 904, 50
- Naidu R. P. et al., 2022, *MNRAS*, 510, 4582
- Nakajima K., Ouchi M., 2014, *MNRAS*, 442, 900
- Oesch P. A. et al., 2016, *ApJ*, 819, 129
- Osterbrock D. E., Ferland G. J., 2006, *Astrophysics of Gaseous Nebulae and Active Galactic Nuclei*. University Science Books; 2nd edition, Sausalito, United States
- Pahl A. J., Shapley A., Steidel C. C., Chen Y., Reddy N. A., 2021, *MNRAS*, 505, 2447
- Pâris I. et al., 2018, *A&A*, 613, A51
- Pearson W. J. et al., 2019, *A&A*, 631, A51
- Pilyugin L. S., Thuan T. X., 2005, *ApJ*, 631, 231
- Planck Collaboration VI, 2020, *A&A*, 641, A6
- Reddy N. A., Steidel C. C., 2009, *ApJ*, 692, 778

- Rivera-Thorsen T. E. et al., 2017, *A&A*, 608, L4
 Rivera-Thorsen T. E. et al., 2019, *Science*, 366, 738
 Robertson B. E., Ellis R. S., Furlanetto S. R., Dunlop J. S., 2015, *ApJ*, 802, L19
 Rojas-Ruiz S., Finkelstein S. L., Bagley M. B., Stevans M., Finkelstein K. D., Larson R., Mechtley M., Diekmann J., 2020, *ApJ*, 891, 146
 Roman-Duval J. et al., 2020, *Res. Notes Am. Astron. Soc.*, 4, 205
 Rubin K. H. R., Prochaska J. X., Koo D. C., Phillips A. C., 2012, *ApJ*, 747, L26
 Rutkowski M. J. et al., 2017, *ApJ*, 841, L27
 Saldana-Lopez A. et al., 2022, *A&A*, 663, A59
 Santini P. et al., 2017, *ApJ*, 847, 76
 Saxena A. et al., 2022, *MNRAS*, 511, 120
 Schaerer D., de Barros S., 2009, *A&A*, 502, 423
 Schaerer D., Izotov Y. I., Verhamme A., Orlitová I., Thuan T. X., Worseck G., Guseva N. G., 2016, *A&A*, 591, L8
 Schaerer D. et al., 2022, *A&A*, 658, L11
 Schlafly E. F., Finkbeiner D. P., 2011, *ApJ*, 737, 103
 Selsing J., Fynbo J. P. U., Christensen L., Krogager J. K., 2016, *A&A*, 585, A87
 Senchyna P., Stark D. P., Charlot S., Chevillard J., Bruzual G., Vidal-García A., 2021, *MNRAS*, 503, 6112
 Shapley A. E., Steidel C. C., Pettini M., Adelberger K. L., 2003, *ApJ*, 588, 65
 Shapley A. E., Steidel C. C., Strom A. L., Bogosavljević M., Reddy N. A., Siana B., Mostardi R. E., Rudie G. C., 2016, *ApJ*, 826, L24
 Sharma M., Theuns T., Frenk C., Bower R., Crain R., Schaller M., Schaye J., 2016, *MNRAS*, 458, L94
 Sharma M., Theuns T., Frenk C., Bower R. G., Crain R. A., Schaller M., Schaye J., 2017, *MNRAS*, 468, 2176
 Shibuya T. et al., 2014, *ApJ*, 788, 74
 Stanway E. R., Eldridge J. J., Becker G. D., 2016, *MNRAS*, 456, 485
 Steidel C. C., Strom A. L., Pettini M., Rudie G. C., Reddy N. A., Trainor R. F., 2016, *ApJ*, 826, 159
 Steidel C. C., Bogosavljević M., Shapley A. E., Reddy N. A., Rudie G. C., Pettini M., Trainor R. F., Strom A. L., 2018, *ApJ*, 869, 123
 Tacchella S., Dekel A., Carollo C. M., Ceverino D., DeGraf C., Lapiner S., Mandelker N., Primack Joel R., 2016a, *MNRAS*, 457, 2790
 Tacchella S., Dekel A., Carollo C. M., Ceverino D., DeGraf C., Lapiner S., Mandelker N., Primack J. R., 2016b, *MNRAS*, 458, 242
 Trainor R. F., Steidel C. C., Strom A. L., Rudie G. C., 2015, *ApJ*, 809, 89
 Valentino F. et al., 2020, *ApJ*, 889, 93
 Vanzella E. et al., 2012, *ApJ*, 751, 70
 Vanzella E. et al., 2016, *ApJ*, 825, 41
 Vanzella E. et al., 2017, *MNRAS*, 465, 3803
 Vanzella E. et al., 2018, *MNRAS*, 476, L15
 Vanzella E. et al., 2020, *MNRAS*, 491, 1093
 Verhamme A., Orlitová I., Schaerer D., Hayes M., 2015, *A&A*, 578, A7
 Verhamme A., Orlitová I., Schaerer D., Izotov Y., Worseck G., Thuan T. X., Guseva N., 2017, *A&A*, 597, A13
 Williams C. C. et al., 2015, *ApJ*, 800, 21
 Wofford A., Leitherer C., Salzer J., 2013, *ApJ*, 765, 118
 Xu X. et al., 2022, *ApJ*, 933, 202
 Yung L. Y. A., Somerville R. S., Finkelstein S. L., Popping G., Davé R., 2019, *MNRAS*, 483, 2983
 Zackrisson E., Inoue A. K., Jensen H., 2013, *ApJ*, 777, 39
 Zackrisson E. et al., 2017, *ApJ*, 836, 78
 Zolotov A. et al., 2015, *MNRAS*, 450, 2327

This paper has been typeset from a $\text{\TeX}/\text{\LaTeX}$ file prepared by the author.